Dissertationes Forestales 372

Laser scanning for tree growth measurements: linking growth patterns to species and wood properties

Maryam Poorazimy

School of Forest Sciences
Faculty of Science, Forestry and Technology
University of Eastern Finland

Academic dissertation

To be presented, with the permission of the Faculty of Science, Forestry and Technology of the University of Eastern Finland, for public criticism in the auditorium N100 of the University of Eastern Finland, Yliopistokatu 7, Joensuu, on the 26th of June 2025, at 12 p.m.

Title of dissertation: Laser scanning for tree growth measurements: linking growth patterns to species and wood properties
Author: Maryam Poorazimy

Dissertationes Forestales 372
https://doi.org/10.14214/df.372

Thesis Supervisors:
Professor Mikko Vastaranta
School of Forest Sciences, University of Eastern Finland, Finland

Senior Researcher, Docent Ninni Saarinen
School of Forest Sciences, University of Eastern Finland, Finland

University Research Fellow, Docent Ville Kankare
Department of Geography and Geology, University of Turku, Finland

Postdoctoral Researcher Tuomas Yrttimaa
School of Forest Sciences, University of Eastern Finland, Finland

Pre-examiners:
Professor Ruben Valbuena
Department of Forest Resource Management, Swedish University of Agricultural Sciences, Sweden

Associate Professor Ole Martin Bollandsås
Faculty of Environmental Sciences and Natural Resource Management, Norwegian University of Life Sciences, Norway

Opponent:
Research Team Leader, Doctor Jussi Peuhkurinen
VTT Technical Research Center of Finland Ltd, Finland

ISSN 1795-7389 (online)
ISBN 978-951-651-834-6 (pdf)

Publishers:
Finnish Society of Forest Science
Faculty of Agriculture and Forestry of the University of Helsinki
School of Forest Sciences of the University of Eastern Finland

Editorial Office:
Finnish Society of Forest Science
Viikinkaari 6, FI-00790 Helsinki, Finland
http://www.dissertationesforestales.fi

Poorazimy M. (2025). Laser scanning for tree growth measurements: linking growth patterns to species and wood properties. Dissertationes Forestales 372. 56 p. https://doi.org/10.14214/df.372

ABSTRACT

The wood properties of standing trees are usually measured through destructive sampling, which is laborious and limited in terms of the number of observations that can be collected across a range of forest structures. In this thesis, the potential of bi-temporal laser scanning (LS) was explored to address these limitations by establishing a link between wood properties and the development of external tree characteristics. This thesis is an amalgamation of Studies **I**–**III**, in which all the experiments were conducted at the Evo study site in Southern Finland, encompassing diverse boreal forests.

Study **I** assessed the feasibility of detecting increments in crown metrics using bi-temporal airborne LS (ALS) acquired over a 5-year time interval. Significant increments were obtained across different crown metrics, the most prominent being recorded for crown volume and crown surface area. Differences were also noted between tree species in relative increments of the crown metrics, with Scots pine (*Pinus sylvestris* L.) differing significantly from Norway spruce (*Picea abies* [L.] H. Karst.) and birch (*Betula* spp.), though species still accounted for a small portion of variability.

The increments in tree height and crown metrics observed over a 7-year monitoring period, in addition to their initial state, were then used to explain stem volume growth (ΔV) in Study **II**. To avoid point cloud occlusion, which typically occurs when the data is acquired using either aerial or terrestrial platforms, a combination of helicopter-borne ALS and terrestrial LS point clouds was used for the tree observations. Scots pine showed the highest associations between ΔV and tree height, crown projection area, and crown perimeter. By contrast, increments in crown volume and crown surface area emerged as highly important metrics for predicting the ΔV of Norway spruce and birch using random forest regression.

Building on these findings, Study **III** addressed the use of bi-temporal ALS for assessing wood properties and their variations between the trees and stands represented by the sample plots. Wood properties were measured using X-ray microdensitometry over 15 growing seasons corresponding with ALS acquisitions. It was demonstrated that the mean annual increment in tree height was moderately associated with mean ring width across all species at both levels of the tree ($RW_{mean-tree}$) and sample plot ($RW_{mean-plot}$). In turn, basal area weighted mean wood density showed limited associations with the growth metrics, with only Scots pine yielding significant models at both levels of the tree ($WD_{mean-tree}$) and sample plot ($WD_{mean-plot}$). However, accounting for plot-level variability in linear mixed-effect regression improved the explanatory power of both the $WD_{mean-tree}$ and $RW_{mean-tree}$ models at the tree level.

Overall, this thesis contributes to the current knowledge by demonstrating the feasibility of utilizing bi-temporal point clouds to characterize increments in tree and crown metrics. It provides insights into methodologies for assessing growth allocation and highlights the potential of tree and crown metrics to explain wood properties and their variations non-destructively and repeatedly.

Keywords: Ring width, Growth, Terrestrial laser scanning, Wood density, Tree crown, Time series

ACKNOWLEDGMENTS

I would like to express my heartfelt gratitude to everyone who has supported me throughout this PhD journey. First and foremost, I would like to thank my main supervisor, Mikko Vastaranta, for his support and inspiration. I also extend my appreciation to my co-supervisors, Ninni Saarinen, Ville Kankare, and Tuomas Yrttimaa for their invaluable input and guidance. This research was made possible through the financial support of the Research Council of Finland, specifically via the following projects "Forest–Human–Machine Interplay Flagship of Science, Understanding Wood Density Variation Within and Between Trees Using Multispectral Point Cloud Technologies and X-ray Microdensitometry, and the Measuring Spatiotemporal Changes in Forest Ecosystem Research Infrastructure." I am grateful to Professor Ruben Valbuena and Associate Professor Ole Martin Bollandsås for their thoughtful pre-examination. I also extend my warm thanks to Research Team Leader, Dr. Jussi Peuhkurinen for kindly accepting the role of opponent and contributing to the public examination. I would like to thank everyone involved in the field campaigns, especially Reinis Cimdins and Antti Polvivaara for collecting the wood samples. A special thanks goes to Ghasem Ronoud for his unwavering help, patience, and support. I truly could not imagine this journey without him. Finally, I would like to thank my dear family for their endless love and unconditional support.

Helsinki, October 2024

Maryam Poorazimy

LIST OF ORIGINAL ARTICLES

This thesis is based on findings presented in the following articles, referred to by the Roman Numerals I–III.

I Poorazimy M, Ronoud G, Yu X, Luoma V, Hyyppä J, Saarinen N, Kankare V, Vastaranta M (2022) Feasibility of bi-temporal airborne laser scanning data in detecting species-specific individual tree crown growth of boreal forests. Remote Sensing 14(19):4845. https://doi.org/10.3390/rs14194845

II Poorazimy M, Ronoud G, Yrttimaa T, Luoma V, Bianchi S, Huuskonen S, Hyyppä J, Saarinen N, Kankare V, Vastaranta M (In review) Understanding tree growth dependencies using multisensorial point clouds. European Journal of Forest Research. Manuscript

III Poorazimy M, Ronoud G, Yrttimaa T, Hyyppä J, Saarinen N, Kankare V, Vastaranta M (2024) An integrated approach combining bi-temporal airborne laser scanning and X-ray microdensitometry in assessing wood properties. Forest Ecology and Management 585:122497. https://doi.org/10.1016/j.foreco.2025.122497

AUTHOR’S CONTRIBUTIONS

I Poorazimy participated in planning the study together with her supervisors, processed the datasets, conducted all the analyses, and wrote the first draft of the manuscript.

II Poorazimy participated in planning the study together with her supervisors, conducted all the analyses, and wrote the first draft of the manuscript.

III Poorazimy participated in planning the study together with her supervisors, processed the datasets, conducted all the analyses, and wrote the first draft of the manuscript.

TABLE OF CONTENTS

1 INTRODUCTION **11**
1.1 Wood properties and their variation in forests 11
1.2 The use of laser scanning in characterizing tree crowns and their growth 13
1.3 Objectives 17
2 MATERIALS AND METHODS **17**
2.1 Study area and field measurements 17
2.2 X-ray microdensitometry measurements 20
2.3 Point cloud data 22
2.4 Pre-processing point cloud data 24
2.5 Point cloud data processing 24
2.6 Characterizing individual trees into tree and crown metrics 27
2.7 Tree-to-tree matching to calculate increments in the tree and crown metrics 28
2.8 Statistical analysis and accuracy assessment 30
3 RESULTS **32**
3.1 Feasibility of bi-temporal ALS data in detecting increments in crown metrics (Studies I and II) 32
3.2 The relationship between stem volume growth and crown metrics, including their increments characterized by multisensorial point clouds (Study II) 35
3.3 The relationship between wood properties and ALS-derived increments in crown metrics (Study III) 37
4 DISCUSSION **39**
4.1 Feasibility of point clouds in the detection of increments in crown metrics as well as species-specific differences 39
4.2 Explaining species-specific stem volume growth 40
4.3 Assessing wood properties and their variations 42
5 CONCLUSION **44**
REFERENCES **45**

ABBREVIATIONS

3D	three-dimensional
ALS	airborne laser scanning
CA	crown projection area
CD	crown width
CHM	canopy height model
CH_{min}	crown base height
CP	crown perimeter
CP/CA	crown perimeter to crown projection area ratio
CSA	crown surface area
CSA/CV	crown surface area to crown volume ratio
CV	crown volume
dbh	diameter at breast height
H	tree height
Heli-ALS	helicopter-borne laser scanning
LS	laser scanning
GNSS	Global Navigation Satellite System
IMU	Inertial Measurement Unit
LMER	linear mixed effect regression
LMF	local maxima filter
MLR	multiple linear regression
r	correlation
R^2	coefficient of determination
R^2_c	conditional coefficient of determination
R^2_m	marginal coefficient of determination
RANSAC	random sample consensus
RF	random forest
RMSE	root mean square error
rRMSE	relative root mean square error
RW	ring width
RW_{mean_plot}	plot-level mean of individual trees mean ring width
RW_{mean_tree}	individual tree mean ring width
RW_{std_plot}	plot-level standard deviation of individual trees mean ring width
rΔC	relative growth in crown metrics
TLS	terrestrial laser scanning
UAV-LS	unmanned aerial vehicle-laser scanning
V	stem volume
WD	wood density
WD_{mean_plot}	plot-level mean of individual trees basal area-weighted mean wood density
WD_{mean_tree}	individual tree basal area-weighted mean wood density
WD_{std_plot}	plot-level standard deviation of individual trees basal area-weighted mean wood density
Δ	growth in tree metrics
ΔC	growth in crown metrics
ΔC_{mean_plot}	plot-level mean of individual trees mean annual growth in crown metrics

ΔC_{mean_tree}	individual tree mean annual growth in crown metrics
ΔC_{std_plot}	plot-level standard deviation of individual trees mean annual growth in crown metrics
ΔH	growth in tree height
ΔH_{mean_plot}	plot-level mean of individual trees mean annual growth in tree height
ΔH_{mean_tree}	individual tree mean annual growth in tree height
ΔH_{std_plot}	plot-level standard deviation of individual trees mean annual growth in tree height
ΔV	growth in stem volume
η^2	generalized eta squared

1 INTRODUCTION

1.1 Wood properties and their variation in forests

Sustainable forest management requires the recognition of competing ecosystem services, including timber production, water regulation, carbon sequestration, and the preservation of biodiversity (Van Leeuwen et al. 2011; Wylie et al. 2019). To manage and use forest resources effectively, we need knowledge about the structure of trees and forests, wood properties, and how these characteristics develop under different growth conditions. Growing wood with desired properties is among the key goals in forest management. The desired wood properties, however, may vary according to the specific end product. For instance, the most important wood properties for the timber industry are wood density (WD), the proportions of heartwood and sapwood, and the size, type, and placement of knots, with fiber length, wood-cell properties, and chemical compositions being most relevant for the pulp and paper industries (Listyanto and Nichols 2009). Silvicultural treatments aim to control the growth patterns and resulting tree form that lead to the variability in wood properties, influencing its suitability for end use (Barrette et al. 2023). In intensive forest management, for example, aimed at maximizing wood and timber production, these treatments include thinning, pruning, fertilization, and the removal of competing vegetation (Barrette et al. 2023). However, due to the acceleration of the formation of earlywood rather than latewood, wood properties are also changed deleteriously in terms of WD, stiffness, and strength (Barrette et al. 2023; Moore and Cown 2017). Wood properties are also influenced more by species-specific morphological plasticity and stand structure than species mixing, which is often higher in mixed and uneven-aged stands (Pretzsch and Rais 2016). Hence, understanding the drivers of variation in wood properties is essential to anticipate the effect of forest management on future wood supplies. This knowledge has economic implications in terms of increasing the productivity of the supply chains.

Wood properties are known to vary by species, wood anatomical structure, tree, stand, and site characteristics, which make them complex to assess. Throughout the stem, variations in the relative amount of cell types, cell dimensions, and chemical compositions determine the wood's properties. These include supra-cellular and sub-cellular characteristics, such as ring width (RW), WD, the proportions of sapwood and heartwood, and the proportions of juvenile and mature wood, in addition to cell length, microfibril angle, and cell-wall thickness. Wood properties can also vary in response to individual tree characteristics, such as crown structure, branch architecture, knot size, knot placement, tree height (H), diameter, and stem taper (Duchesne et al. 1997; Krajnc et al. 2019; Kuprevicius et al. 2013; Mäkinen and Colin 1998). On a broader scale, competition between trees, stocking density, and disturbances have profound effects on wood quality as stand-level extrinsic characteristics (Ikonen et al. 2008; Kankare et al. 2022). All of these also change with tree age and stand development (Van Leeuwen et al. 2011; Wylie et al. 2019).

The most common species-specific wood property that has been studied over the years is WD (Downes and Drew 2008). This mostly defines the value of the wood structure, in terms of stiffness and pulp yield, and plays a key role in tree-level hydraulic efficiency and mechanical support (Demol et al. 2021; Swenson and Enquist 2007; Van Leeuwen et al. 2011). It also directly affects tree biomass and carbon content predictions as a crucial conversion factor in transforming volume into biomass (Demol et al. 2021; Pokharel et al.

2016; Van Leeuwen et al. 2011; Wylie et al. 2019). The cell-wall thickness, ratio of latewood to earlywood, and tracheid size and shape determine WD variation, which is also dependent on the seasons, geographical area, and site conditions (Demol et al. 2021; Van Leeuwen et al. 2011). Another intrinsic metric of wood properties that represents the annual growth layer of a tree is RW. This has received particular attention in dendrochronology and growth-pattern studies (Ahmed et al. 2024; Jevšenak et al. 2024). Environmental variables, such as temperature, precipitation, and soil quality, in addition to tree-specific characteristics, such as genetics and competition, influence RW. These factors together determine the annual variations in RW, providing insights into the tree's growth history and the environmental conditions it has experienced (Van Leeuwen et al. 2011). The advancement of measurement technologies and the increasing need for understanding within- and between-tree wood properties serve as the primary motivations driving studies in this area (Downes and Drew 2008). Recently, wood properties have been measured using X-ray microdensitometry systems in the radial and tangential planes (Downes and Drew 2008; Peltola et al. 2007; Schimleck et al. 2019). This allows wood properties to be measured at a relatively high resolution, and not only as an average, but also at the level of the variations typically along a pith-to-bark transect. These X-ray microdensitometry systems combine densitometric measurements with multi-element analysis through X-ray fluorescence. However, these methods are expensive and labor-intensive because wood samples need to be collected, whereas understanding wood properties across a broad range of stand and tree communities is needed urgently for effective forest management and wood procurement (Van Leeuwen et al. 2011). In addition, standard methods of sampling are required to resolve annual growth reliably, especially for species without strong seasonal variation (Downes et al. 1997). Almost infinite sets of growing conditions and silvicultural treatments also affect wood samples, which makes modeling a challenging task.

Tree crown characteristics affect wood suitability for end-use products by indicating the number of knots in the timber and have been widely used in modeling wood formation and predicting wood quality (Van Leeuwen et al. 2011). According to the conceptual model proposed by Larson (1969), the auxin that is produced in the stem apex has a fundamental role in forming the xylem properties. A higher auxin concentration leads to large-dimeter, thin-walled earlywood cells. Hence, earlywood production declines as distance from the auxin-producing live crown increases, with trees with large crowns being likely to produce wood with inferior mechanical wood properties. Crown dimensions, which are regulated in response to the stand density and competition status, can affect the wood interior characteristics (Van Leeuwen et al. 2011). This relationship is dependent on the competitive status of the crown (dominant, co-dominant or suppressed), as well as the shade tolerance of the studied species (Amarasekara and Denne 2002; Chen et al. 2017). Mechanical loading of the crown, which redistributes growth to the high-stress region, is another factor affecting the xylem properties (Krajnc et al. 2019).

Previous studies have shown it is possible to assess stem growth by means of crown characteristics and their development over time (Pretzsch 2021; Seidel et al. 2015; Yrttimaa et al. 2022). Tree crown and stem growth are structurally and functionally linked to each other. The stem holds up the tree crown by hydraulics and mechanical supplies and transports water and nutrients to the leaves through the vessel elements. Conversely, the tree crown translocates photosynthetic carbon to the stem. These two features retain similar information and have been used in many eco-physiological growth models in combination with each other (Pretzsch 2021; Sievänen et al. 2000). Krajicek et al. (1961) were among the first to determine the relationship between crown width and stem diameter at breast height (dbh) in open-grown trees. Understanding these species-specific relationships can also be used to assess species tolerance to variations in stand density, guide thinning treatments, and estimate growth. For instance, Mitchell (1969) used this simple relationship for a tree growth model in white spruce (*Picea glauca* [Moench.] Voss). Also, Mitchell (1975) demonstrated how to relate stem growth and crown dimension in Douglas-fir (*Picea menziesii* [Mirb.] Franco), using the resulting growth model in a simulation system for the silviculture of Douglas fir. In another study, Ottorini et al. (1996) developed an equation to estimate annual stem volume growth using stem and crown characteristics in even-aged ash (*Fraxinus excelsior* L.) stands. They showed that foliar volume—a product of crown projection area and annual height growth—along with its relative measure, computed as a ratio between foliar volume and stem surface area raised to the power of 3/2, were the determining factors in stem growth of ash stands. A larger tree crown usually needs a bigger stem to support the increased biomass, thus establishing a link between the tree crown and RW. This is important in the context of metabolic scaling theory, which predicts the scaling up of photosynthetic and metabolic rates with biomass growth (Ahmed and Pretzsch 2023). Quantifying this link is also important because it reflects the impacts of past management actions.

However, measuring tree crown dimensions is time-consuming and difficult in the field due to their inaccessibility. Sometimes, simpler measures can be applied, such as tree dbh, height, and age for predicting competition between trees and their wood properties, but this method includes uncertainties (Biging and Dobbertin 1995; Ma et al. 2018; Van Leeuwen et al. 2011; Wensel et al. 1987). In permanent sample plots that enable forest monitoring, recording the development of trees requires the ability to relocate and remeasure specific trees, which is again time-consuming and prone to measurement errors. In addition, crown properties are rarely monitored. In general, the variability in consecutive measurements of trees and forests poses a challenge in distinguishing between the contributions of actual changes and measurement errors, especially when the magnitude of the actual change falls within the accuracy limits of the measurement technique. For instance, Luoma et al. (2017) assessed the repeatability of field measurements of dbh and height using calipers and clinometers in four independent measurements of 319 sample trees. They achieved a standard deviation of 1.5% for the dbh and 2.9% for the height measurements. Quantifying the structure of the crown is destructive and labor-intensive if the trees are felled, and detailed measurements of branch characteristics must be conducted to calculate the position, length, and angle of the branches relative to the initiation point of each annual stem growth unit (Ottorini et al. 1996; Seifert 2003).

1.2 The use of laser scanning in characterizing tree crowns and their growth

Laser scanning (LS) is an active remote-sensing technique that utilizes laser pulses for directed range measurements, and is capable of reconstructing the three-dimensional (3D) structures of trees and stands in a digital format as point clouds (Wehr and Lohr 1999). This can be deployed from static or mobile, aerial or terrestrial platforms. Over the last decade, this method has revolutionized forestry research and operations by integrating airborne LS (ALS) into forest inventory practices (Maltamo et al. 2006; Næsset 2004; White et al. 2017).

Typically, ALS provides observations of vegetation height and density with a wide geographical coverage (White et al. 2017). Previous studies have shown its capabilities in characterizing the vertical structure of forests (Coops et al. 2007; Hyyppä et al. 2008; Zhao et al. 2018). Particularly, ALS has been demonstrated to be a promising technique for the mapping and monitoring of tree crowns (Duncanson and Dubayah 2018; Popescu and Zhao 2008). For instance, Frew et al. (2016) used the manual detection of individual trees to determine the crowns of Douglas fir (*Pseudotsuga menziesii* [Mirb.] Franco var. *menziesii*) trees at multiple time points. This manual detection was based on points of interest representing the location of individual trees in the field, discrete ALS datasets, and four-band multispectral imagery. They used FUSION software to subset the ALS data and multispectral imagery by zooming into field points of interest in an interactive viewer, allowing visual identification of the point clouds associated with individual trees. These were further processed interactively to calculate H and crown metrics, such as base height. The crown volume (CV) of individual trees was also obtained by triangulating the exterior crown points into a convex hull. The results showed a significant mean difference between ALS-derived H and crown base height with field measurements at a 95% confidence interval, resulting in coefficient of determination (R^2) values of 0.98 and 0.79, respectively. Similar results were obtained between the predicted field and ALS-derived CVs, with an R^2 value of 0.45 compared to the field-measured CV.

Terrestrial LS (TLS) is generally considered a non-destructive technology that provides detailed point clouds enabling millimeter-level details in the 3D characterization of individual trees, particularly the stem characteristics (Calders et al. 2020; Kankare et al. 2014; Liang et al. 2014; Liu et al. 2018; Srinivasan et al. 2015; Yrttimaa et al. 2020b). It has also been successfully applied in the characterization of tree crowns and branching structures (Metz et al. 2013; Srinivasan et al. 2015; Yrttimaa et al. 2024). Compared to ALS, TLS covers smaller, localized areas because its extent is limited by the static platform and hemispherical measurement geometry (Liang et al. 2016). Hence, TLS measurements are increasingly used nowadays as a reference for assessing how well other approaches are capable of measuring stem dimensions and crown properties. For example, in Jung et al. (2011), the tree and crown metrics of 15 Korean pines (*Pinus koraiensis*), extracted from ALS, were assessed using TLS data collected from the cardinal directions and manually processed into individual trees to obtain their characteristics, whereas the ALS data were segmented into individual tree crowns using the iterative watershed method, with the extended maxima transformation of image processing corresponding to each field-measured tree. Then, the H, crown projection area (CA), and CV were obtained for each segmented crown. They also estimated the crown base height through the iterative *k*-means clustering algorithm. The results of a regression analysis between the estimates of ALS and TLS resulted in R^2 values of 0.94, 0.75, 0.69, and 0.58 for the H and CA, geometric volume, and base height, respectively.

However, the capabilities of ALS and TLS in characterizing tree crown structures are limited in dense forests, where the crowns of individual trees overlap (Jung et al. 2011; Metz et al. 2013; Srinivasan et al. 2015; Weiner 2004). The below-canopy viewpoint of TLS reduces the visibility of crown structures toward the top of the canopy, which are often occluded by the crowns of adjacent trees (Liang et al. 2018). This limited coverage of TLS point clouds at the top of the canopy is typically mitigated by adopting a multiscan approach during data acquisition and using scanners capable of recording multiple returns for each laser signal emitted. However, capturing the vertical structure of trees remains challenging in closed-canopy conditions, and can lead to underestimations of H (Liang et al. 2018; Vaglio Laurin et al. 2019) in addition to the inaccurate characterization of the crown dimensions and the competitive status of the trees (Terryn et al. 2022). A complementary viewpoint from the upper part of the canopy can be provided by ALS, but at the cost of the horizontal structure and stem dimensions, which are occluded by the canopy vegetation (Polewski et al. 2019; Terryn et al. 2022). Kükenbrink et al. (2017) quantified the occluded canopy volume of ALS over part of a semi-natural mixed deciduous forest in Zurich, Switzerland, using a voxel traversal algorithm. They also analyzed the dependency of occluded canopy volume on pulse density, flight-strip overlap, and acquisition season. The results showed that, even with the highest average pulse density (11 pulses/m^2), at least 25% of the canopy volume remained occluded in the ALS acquisitions under leaf-on conditions. Roughly 7% of this occlusion was recovered by combining the leaf-off and leaf-on acquisitions. A cross-comparison with the TLS acquired for the leaf-on conditions further revealed that 28% of the vegetation elements detected by TLS were not detected by ALS due to the effects of occlusion. They also found a significant increase in the amount of observed canopy volume with larger flight-strip overlap. In a study by Novotny et al. (2021), the accuracy of individual tree attributes measured by ALS and TLS was affected by the occlusion primarily using the automatic segmentation method. However, the manual segmentation method was also partly influenced by complex forest structure and subjective evaluation. The scanned H had the highest correlation (r) with the field-measured H for Norway spruce (*Picea abies* [L.] H. Karst.). The correlations were r = 0.91 for ALS automatic segmentation, r = 0.94 for ALS manual segmentation, and r = 0.91 for TLS manual segmentation. The TLS estimates of crown base height were more accurate than the ALS estimates, with the TLS manual segmentation having r = 0.85 with a standard error of 1.4 m. In terms of crown diameter, the ALS manual segmentation showed better agreement with the field measurements than the TLS manual segmentation (r = 0.71).

Hence, the combination of ALS and TLS in a multisensorial framework can potentially lead to a higher level of detail in tree characterization. Panagiotidis et al. (2022) evaluated the efficiency of unmanned aerial vehicle LS (UAV-LS) and TLS separately and in combination in order to estimate individual tree metrics under different management types. The combination of UAV-LS and TLS significantly increased the accuracy of the H and dbh measurements, especially in broadleaves, giving root mean square error (RMSE) values of 0.7 m and 0.9 cm, respectively. They also observed changes in crown structure compared to the separate datasets, which led to improved estimates for all the crown metrics. Yun et al. (2019) provided a quantitative comparison of the occlusion effect among different LS of fixed-position terrestrial, multiple terrestrial, and airborne-terrestrial approaches. In this study, five virtual 3D tree models, based on field measurements from multiple tree crowns, were reconstructed, and multiplatform LS simulations were performed on these. The results showed that the one simulated terrestrial scan captured only 25–38% of the leaf area, which increased to 60–73% when three simulated terrestrial scans around one tree were acquired. Importantly, the inclusion of a supplementary airborne scan reduced the occlusion and recovered 72–90% of the leaf area. A similar result was obtained by Schneider et al. (2019). They compared two measurement setups for tropical and temperate forests, separately, including a combination of TLS and laser scans from a canopy crane, and a combination of TLS and UAV-LS. The results showed it was possible to combine ground and above-canopy measurements to sample the CV with less than 2% occlusion. The sufficient coverage of TLS was observed when no sampling of the leaves and branches at the top of the canopy was required. Contrastingly, UAV-LS and the measurements from canopy cranes showed considerable occlusion in the middle and understory. However, forests with complex structures may benefit more from being characterized using multisensorial point clouds than forests with simpler structures, as discussed in Yrttimaa et al. (2020a). In that study, the estimation accuracies of forest structural attributes, using TLS point clouds and a combination of TLS with photogrammetric point clouds acquired from UAV, were assessed in managed Scots pine stands. These structural attributes were computed by aggregating individual tree observations. They showed that both TLS and its combination with UAV were capable of deriving plot-level stem number, basal area, and basal area weighted mean diameter with relative RMSE (rRMSE) values of less than 4.8% because the TLS alone also captured the upper part of the canopy rather well in simple forest structures. However, the rRMSE values improved from 4.3 to 2.8% for the plot-level basal area weighted mean height and from 6.2 to 5.4% for the plot-level mean stem volume when the combination of TLS and UAV was used.

In addition, the use, availability, and temporal resolution of LS is increasing, allowing us to take advantage of time-series data to observe or model structural changes in trees and forests. Generally, modeling these changes is applied by either direct or indirect methods (McRoberts et al. 2014; Soininen et al. 2024). With the direct method, the change in variables of interest is predicted from the observed changes in multitemporal LS point clouds as direct predictors. The indirect method predicts change by differencing independent predictions of the variable of interest obtained through time. These changes can also be predicted at different spatial scales, divided into canopy-gap-based, area-based, and individual tree-level analyses (Soininen et al. 2024). Unlike the area-based and individual tree-level analyses, the level of detail provided by the canopy-gap-based analysis is very often not clear. In this method, the changes are detected through differencing point-cloud-derived metrics or a canopy height model (CHM) (Noordermeer et al. 2019; Vastaranta et al. 2013). In area-based analysis, metrics describing the horizontal and vertical distributions of pulse returns in a regular, fixed area larger than the tree crowns are used to predict forest changes (Dubayah et al. 2010; Næsset and Gobakken 2005). However, spatial information beyond this area, and harvested or fallen trees at the level of the tree, are lost (Soininen et al. 2022). The addition of detail is provided by individual tree-level analysis, which enables investigation of the relationship between tree growth and other factors, such as tree size, competition, species composition, and stem density. Hence, it simulates attempts to link these measurements with conventional individual tree growth models (Tompalski et al. 2021). This information can also be aggregated at the stand level, although Peng (2000) acknowledged that it does not necessarily correspond to the average change in multilayered forest stands because it is weighted by the dominant trees.

Both ALS and TLS have been demonstrated as being able to quantify tree growth and structural changes if consecutive measurements are collected over time (Luoma et al. 2021; Sheppard et al. 2017; Tompalski et al. 2021). A few studies have also predicted changes in the crowns of individual trees. For instance, Duncanson and Dubayah (2018) studied forest change at the individual tree level by comparing the spatially matched individual crowns from two different ALS acquisitions in a high-biomass forest in California. Across Douglas fir trees, Frew et al. (2016) examined the capability of ALS to detect the growth in CV based on manual detection and field reference data. However, the challenge to accurately predict individual-tree changes in the stem and crown persists. In addition, tree growth is prone to high variability between tree species as an intrinsic source of change because each species responds to lightning conditions, growing space, and resources differently (Coomes and Allen 2007). This emphasizes the need for further species-specific studies under different growing conditions.

1.3 Objectives

The effective management and utilization of forest resources require an understanding of tree and forest structure, wood properties, and the development of these characteristics under various growth conditions. In this thesis, the ability of LS to monitor tree growth patterns in boreal forests was investigated, these measurements being linked to species and wood properties. The following specific objectives and related questions were addressed in Studies **I**–**III**.

The first objective was to investigate the feasibility of bi-temporal ALS data to detect increments in crown metrics (Study **I**), with the related research question (RQ1) formulated around whether increments in the ALS-derived crown metrics could be detected over a 5-year period. If the increments could be detected, the second research question (RQ2) was whether the relative increments in the investigated metrics differed between tree species.

The second objective was to investigate the relationships between stem volume growth and crown metrics, in addition to their increments over time, using a combination of bi-temporal TLS and helicopter-borne ALS point clouds (Study **II**). The related research question (RQ3) was about the extent to which crown metrics and their increments over time explained the observed variation in stem volume growth.

The third objective was to assess wood properties and their variation between trees and sample plots using bi-temporal ALS data (Study **III**). The related research question (RQ4) asked how the basal area weighted mean WD and mean RW were related to the respective ALS-derived mean annual increments in crown metrics at the tree and plot levels, analyzed by species.

2 MATERIALS AND METHODS

2.1 Study area and field measurements

The study area was located in the southern boreal forest of Finland, at Evo (61.19ºN, 25.11ºE) (Figure 1a) and included approximately 2,000 ha of managed forest with elevations ranging from 125 to 185 m above sea level. Scots pine (*Pinus sylvestris* L.), Norway spruce (*Picea abies* [L.] H. Karst.), and silver and downy birches (*Betula pendula* Roth and *Betula pubescens* Ehrh., respectively) were the dominant tree species in the study area, contributing 44.7%, 33.5%, and 21.8% of the total volume, respectively. The experimental setup for Study **I** included 91 rectangular sample plots initially established in 2014 with dimensions of 32 × 32 m (1,024 m^2) (Figure 1b).

At the time of establishment, a tree-by-tree field inventory was conducted for the trees with dbh values exceeding 5 cm. The field inventory included tree species and health status determined based on visual interpretations. The dbh measured using calipers and the height using a Vertex IV clinometer (Haglöf Sweden AB, Långsele, Sweden). These were used to compute the tree-level basal area, considering the cross-sectional area of the trees to be circular and calculating the stem volume using the national species-specific volume equation (Laasasenaho 1982). The sum and basal area weighted mean descriptive statistics of the field plots are presented in Table 1.

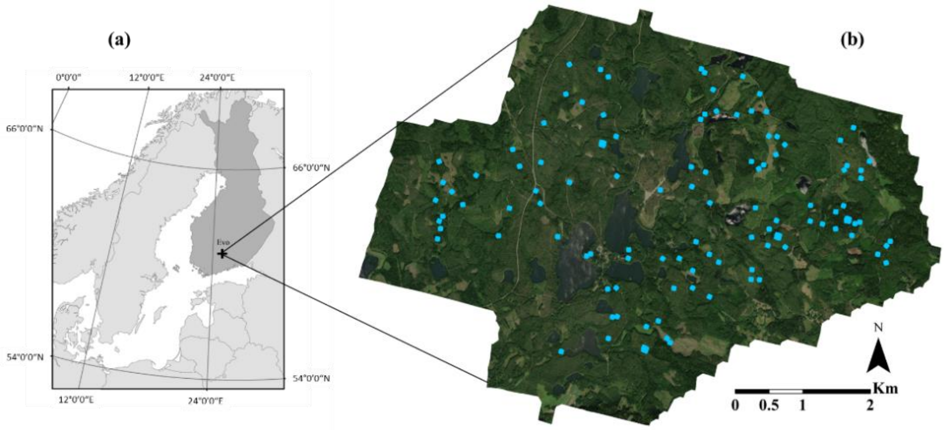

Figure 1. (a) Study area in Evo, Finland, and (b) distribution of sample plots over Esri's world imagery basemap.

Among the 91 sample plots, a subset of 22 sample plots were selected for Study **II**, which encompassed a variety of stand conditions representing different stages of development, species composition, stand density, and canopy layering. These plots have been used to support various remote-sensing research activities, including the international benchmarking of TLS approaches for forest inventory (Liang et al., 2018). The field inventory for these 22 sample plots was repeated in 2021, with the remeasurement of dbh and height of all trees that met the predefined dbh threshold of 5 cm. Table 2 shows the number of trees, stem volume, basal area weighted dbh, and height for all 22 field plots in 2014 and 2021.

Table 1. Summary statistics across the 91 sample plots used in Study **I**, showing the minimum, maximum, mean, and standard deviation of the number of trees, mean volume, basal area weighted mean diameter, and basal area weighted height.

Attribute	Min	Max	Mean	Std.
Number of trees (n/ha)	342	3,076	943	556
Mean volume (m^3/ha)	34.46	518.39	271.49	110.73
Basal area weighted mean dbh (cm)	13.91	46.42	25.79	7.51
Basal area weighted mean height (m)	10.02	31.09	21.10	4.42

Table 2. Summary statistics across the 22 sample plots used in Study **II** for the years 2014 (T1) and 2021 (T2), including minimum, maximum, mean, and standard deviation values for the number of trees, stem volume, basal area weighted dbh, and height.

Attribute	2014				2021			
	Min	Max	Mean	Std.	Min	Max	Mean	Std.
Number of trees (n/ha)	430	3,008	1,238	731	430	2568	1,197	674
Mean volume (m^3/ha)	110.64	482.33	297.24	115.21	143.89	537.24	356.42	117.14
Basal area weighted mean dbh (cm)	13.91	41.58	25.93	9.10	16.08	42.41	27.91	8.79
Basal area weighted mean height (m)	13.03	27.04	21.01	4.14	14.80	28.14	22.50	3.80

For Study **III**, a subset of 59 sample plots, dominated by pines and spruces, was utilized. Trees identified during field measurements in 2014 were considered as the population for wood sampling. In April–May 2023, wood samples were collected from Scots pine and Norway spruce trees using an increment borer at a fixed height of 1.30 m above the ground (Figure 2). The number of samples was determined based on the dominant tree species per plot. Excluding the birch-dominated plots, the number of samples was supposed to be eight for the Scots pine- and Norway spruce-dominated plots and 12 when the species shared more than 30% of the basal area proportion. The selection of sample trees per plot included those located within an 11-m distance from the plot center and with a height exceeding 80% of the dominant height in that plot. This was done to increase the likelihood of detecting these trees in the ALS data. Additionally, sample trees were distributed among different dbh classes and plot sectors spanning 90°, with the main cardinal point sitting at the middle of each, representing various trees and stand conditions. A total of 273 Scots pine and 150 Norway spruce wood samples were collected.

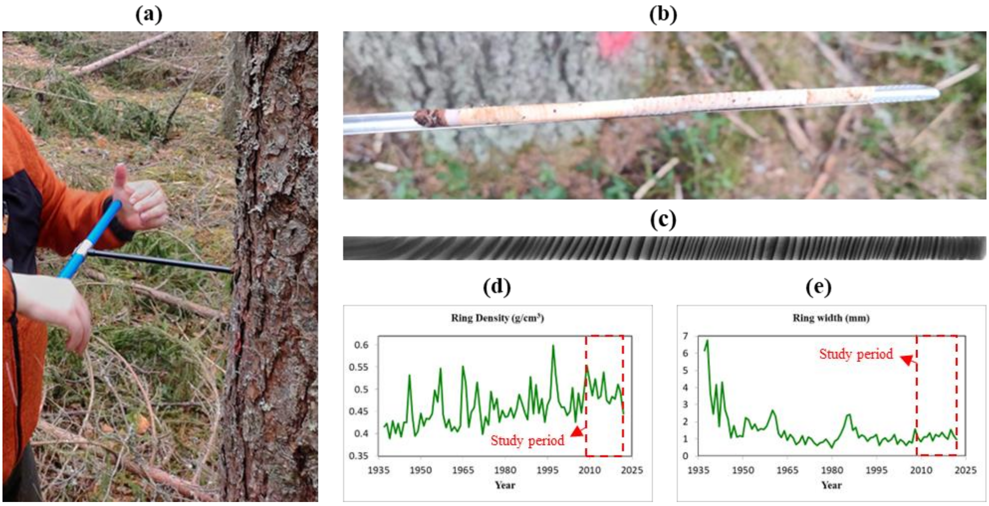

Figure 2. (a) Wood sampling using an increment borer. (b) The core extracted from the tree, and (c) the digital radiographic image generated by X-ray microdensitometry. The resulting (d) WD and (e) RW profiles spanning the tree's lifetime. The red dashed line represents the period investigated in this study.

2.2 X-ray microdensitometry measurements

The reference measurements of wood properties used in Study **III** were obtained using the ITRAX X-ray microdensitometry system (Figure 3) (Cox Analytical Systems, Göteborg, Sweden). First, air-dried samples with a 12% moisture content were scanned in batch mode with a standard X-ray intensity for an exposure time of 20 ms, which generating digital radiographic images with horizontal and vertical pixel sizes of 25 µm. Second, WD profiles were extracted from scanned images using density software (Bergsten et al. 2001), and intra-ring standard measurements were extracted using in-house-developed Excel macros. Based on these, the sample trees' mean WD (WD_{mean_tree}) and RW (RW_{mean_tree}) values for the years 2009 to 2022, which coincided with the ALS acquisitions used in Study **III**, were calculated by species (Subsection 2.3). We omitted the possible early season of 2023 to maintain measurement consistency. The WD_{mean_tree} was weighted by basal area using RW as a proxy for basal area growth from the pith outward (Biondi and Qeadan 2008). At the plot level, the WD_{mean_tree} and RW_{mean_tree} values of individual trees were averaged for each species separately (WD_{mean_plot}, RW_{mean_plot}), and the standard deviation between these was calculated for only the sample plots having at least three observations per species (WD_{std_plot}, RW_{std_plot}). Table 3 summarizes the attributes obtained from the X-ray microdensitometry.

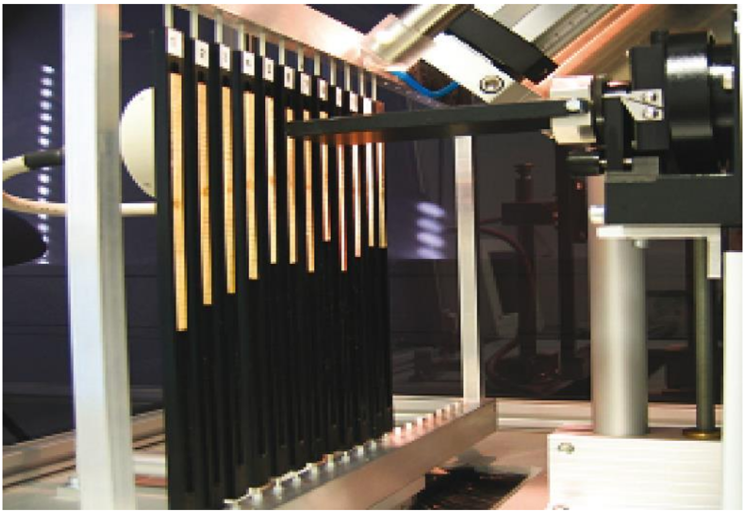

Figure 3. The ITRAX X-ray microdensitometry system (left) developed by Cox Analytical Systems (Peltola et al. 2007).

Table 3. X-ray microdensitometry measurements at the tree and sample plot levels. These include the basal area weighted mean wood density (WD_{mean_tree}) and mean ring width (RW_{mean_tree}) between T1 (2009) and T2 (2023) and their plot-level means (WD_{mean_plot}, RW_{mean_plot}) and standard deviations (WD_{std_plot}, RW_{std_plot}). The minimum, maximum, mean, and standard deviation are presented.

	Min	**Max**	**Mean**	**Std.**
	Tree-level statistics for Scots pine/Norway spruce sample trees (n = 273/150)			
WD_{mean_tree} (g/cm³)	0.42/0.34	0.69/0.57	0.54/0.45	0.05/0.05
RW_{mean_tree} (mm)	0.28/0.28	2.53/3.18	1.26/1.24	0.46/0.51
	Statistics of the mean values for Scots pine/Norway spruce-dominated sample plots (n = 45/25)			
WD_{mean_plot} (g/cm³)	0.44/0.40	0.60/0.49	0.54/0.45	0.03/0.02
RW_{mean_plot} (mm)	0.43/0.50	2.44/2.06	1.25/1.26	0.37/0.41
	Statistics of the standard deviation values for Scots Pine/Norway spruce-dominated sample plots (n = 39/23)			
WD_{std_plot} (g/cm³)	0.01/0.02	0.09/0.08	0.04/0.05	0.02/0.02
RW_{std_plot} (mm)	0.04/0.10	0.62/0.86	0.33/0.37	0.13/0.18

2.3 Point cloud data

All the studies were conducted utilizing point cloud data collected at two distinct time points, referred to as the first (T1) and second (T2) acquisitions. Table 4 provides an overview of the point cloud data used in the studies. Studies **I** and **III** relied solely on ALS data, with T1 acquisition taking place in July 2009, using a Leica ALS-50II SN058 scanner (Leica Geosystems, St. Gallen, Switzerland) with a 30º scanning angle, beam divergence of 0.22 mrad, and wavelength of 1064 nm (hereafter referred to as ALS 2009). The flying altitude was 400 m, with a pulse rate of 150 kHz, resulting in an average point density of 10 pts/m^2. The T2 acquisition for Study **I**, with a lower point density, was collected in September 2014 using a Leica ALS70-HA SN7202 scanner at a scanning angle of 30º and beam divergence of 0.15 mrad (ALS 2014). The pulse rate and flying altitude were 240 kHz and 900 m, resulting in a point density of approximately 6 pts/m^2. In Study **III**, however, the T2 acquisition was collected using a helicopter-borne Riegl VUX-1HA (Riegl Laser Measurement Systems GmbH, Salzburg, Austria) laser scanner in June 2023 (hereafter referred to as ALS 2023). With a flying altitude of 100 m, a flying speed of 50 km/h, and a scanner operating at a pulse rate of 1,017 kHz and a wavelength of 1,550 nm, the data represented an average point density of 1,182 pts/m^2. This scanner is one of the three Riegl scanners in the HeliALS-TW triple-wavelength laser scanning system, which was mounted at the front of the system, with a nominal scan plan of 15º forward, and provided a linear scanning pattern.

A multisensorial framework was applied in Study **II**, combining TLS and ALS at each time point. The helicopter-borne scanner of Riegl VQ-480-U, with a 1,550-nm wavelength, was used for the T1 acquisition of ALS in December 2014 (hereafter referred to as Heli-ALS 2014). This is a lightweight scanner that was operated at a 550-kHz pulse rate and a beam divergence of 0.3 mrad. With a flying altitude of 75 m and a flying speed of 50 km/h, this setup resulted in a point density of approximately 450 pts/m^2. The T2 ALS acquisition for Study **II** was conducted in June 2021 using the multispectral HeliALS-TW system, as used in Study **III**, as mentioned above (hereafter referred to as Heli-ALS 2021). The acquisition took place at a flying altitude of 80 m and a target flying speed of 50 km/h. The combined point cloud data from all the Riegl scanners used, including a VUX-1HA, a MiniVUX-3UAV, and a VQ-840-G, were examined in Study **II**, and featured a point density of 3,200 pts/m^2 and a point spacing of 2.0 cm on the ground. The MiniVUX-3UAV has a linear scanning pattern (120º), similar to the VUX-1HA scanner (360º), whereas the VQ-840-G provides conical scanning principles, with a 40º cone angle. The wavelengths for the MiniVUX-3UAV and the VQ-840-G were 905 and 532 nm, with pulse rates of 300 and 200 kHz, respectively.

The T1 acquisition of TLS for Study **II** occurred in April–May 2014 using a Leica HDS6100 phase-shift scanner (hereafter referred to as TLS 2014). This used a wavelength of 690 nm and provided a 310º vertical × 360º horizontal field of view, with a 0.018º angular resolution and a beam divergence of 0.22 mrad. A total of five individual scans per sample plot were collected to capture a comprehensive point cloud representing the entire sample plot. The center scan was located at the plot center, while the other four auxiliary scans were evenly positioned at an 11.3-m distance around the sample plot center in the quadrant directions (i.e., northeast, southeast, southwest, and northwest). For the T2 acquisition of TLS for Study **II**, the time-of-flight scanner of Leica RTC360 3D was used in a data-acquisition campaign that took place in April–May 2021 (hereafter referred to as TLS 2021). The field of view for this scanner was 300º vertical × 360º horizontal. It operated at a wavelength of 1,550 nm and provided an angular resolution of 0.009º and a beam divergence of 0.16 mrad. More specifically, the scan setup for TLS 2021 was densified in comparison with TLS 2014 because of the improved scanner technology (i.e., higher resolution and measurement frequency, meaning shorter scan times per position) and an enhanced knowledge of the best practices in point cloud data acquisition in boreal forest conditions. The scan setup comprised eight auxiliary scans approximately at the plot borders, in addition to the central scan.

Individual scans from each sample plot were registered together, with the aid of six reflective artificial reference targets attached to the trees at a height of approximately 2 m. These targets were evenly distributed on each sample plot, based on their visibility from the center scan locations, with at least three from the auxiliary scan locations. The Z+F LaserControl software for TLS 2014 and Leica Cyclone 3D Point Cloud Processing software for TLS 2021 were used for registration where the point clouds were merged with an accuracy of 2 mm, on average. It is worth mentioning that the location of the reflective artificial reference target was also determined in the TLS 2014 campaign. To accomplish this, two reference points over open areas, either inside or outside the plot, were located using a Trimble R8 global navigation satellite system (GNSS) receiver (Trimble Inc., CA, USA) with a real-time kinematic correction. A survey point was also established near the plot center, using distance and angle from the reference points. Finally, the location of artificial reference targets was determined using a Trimble 5602 DR200 + total station.

Table 4. An overview of the point cloud data used in Studies **I**, **II**, and **III** at different time points.

Study	Number of plots	First acquisition (T1)		Second acquisition (T2)	
		Year	Scanner	Year	Scanner
I	91	2009	Leica ALS50II SN058 (ALS)	2014	Leica ALS70-HA SN7202 (ALS)
II	22	2014	Riegl VQ 480-U (Heli-ALS) Leica HDS6100 (TLS)	2021	Riegl VUX-1HA/ MiniVUX-3UAV/ VQ-840-G (Heli-ALS) Leica RTC360 3D (TLS)
III	59	2009	Leica ALS50II SN058 (ALS)	2023	Riegl VUX-1HA (Heli-ALS)

2.4 Pre-processing point cloud data

All point clouds were first denoised using LAStools software (rapidlasso GmbH, Cliching, Germany) to remove isolated noisy points, and then normalized by transforming height above sea level to height above the ground. For Study **I**, the point clouds were classified into ground and non-ground points by the data provider using TerraScan software. Similarly, we used LAStools software to assign ground and non-ground classes to each point in Studies **II** and **III**. To date, the algorithm developed by Axelsson (2000) is the simplest and most effective algorithm included in most point cloud classifying software. This algorithm works by creating a grid whose size corresponds to the lowest elevation return—the ground point. From these points, a triangulated facet surface is built, with vertices as bare ground points. Then, the vertical distance and angle of points other than those bare ground points are evaluated. Iteratively, the new ground points that meet the filtering criteria are added to the triangulation facet model. It is worth mentioning that all the pre-processing steps in Study **I** were assisted by 3,000 × 3,000-m tiling. And, to avoid empty pixels and poorly shaped triangle surfaces, a 20-m buffer was used around the tiles (Isenburg 2015). Finally, the normalized point clouds in all the studies were clipped using sample plot polygons. However, the sample plot polygons were buffered by 5 m in Studies **I** and **III** to avoid boundary effects.

The airborne platform was integrated with a GNSS and an inertial measurement unit, offering georeferenced point clouds over the study area. Contrastingly, the complementary terrestrial platform performed in the local coordinate system of the sensor. Hence, a co-registration procedure was conducted to combine the point clouds of the georeferenced Heli-ALS with the local TLS in Study **II**. In T1, TLS 2014 was georeferenced to the EUREF-FIN global coordinate system using the locations of artificial reference targets measured in the TLS 2014 field campaign (Subsection 2.3). The co-registration between Heli-ALS 2014 and TLS 2014 in T1 was also manually checked by determining whether the point clouds overlapped from the top and side views. It was further fine-tuned if discrepancies between point clouds in the horizontal plane persisted. However, obtaining acceptable positional accuracy in forest conditions is not always possible, especially in dense forests. Hence, an automatic co-registration method was conducted to co-register Heli-ALS 2021 with TLS 2021 in T2. This method is a rigid transformation consisting of translation and rotation known as canopy density analysis (Dai et al. 2019). The co-registration began by filtering points below 60% of the maximum height in each sample plot from both datasets, leaving the remaining points as the canopy points. Canopy points were also down-sampled into a 5-cm grid to ensure equal spacing between the datasets, and CHMs were generated at a resolution of 40 cm. Using a local maxima filter with variable window size (Pitkänen et al. 2004), the treetops were extracted and used as descriptors (i.e., tie points) for estimating the initial 2D rigid transformation matrix, including translation and rotation along the *z* axis. This method works simultaneously, allowing the determination of similarity in the descriptors and iteratively estimating the transformation matrix until convergence. The iterative closest point algorithm (Zhang 1994) was used for this reason. Finally, the fine-tuned 2D rigid transformation matrix was used for co-registration between the T2 datasets.

2.5 Point cloud data processing

For the individual tree-level analysis, a raster-based marker-controlled watershed algorithm was used in all studies (**I–III**) to segment the individual tree crowns (Meyer and Beucher

1990). In Study **II,** HeliALS CHMs at T1 and T2 with a 40-cm grid were generated from height-normalized point clouds because it was assumed HeliALS would be more capable than TLS to characterize the tops of the tree crowns. However, for Studies **I** and **III**, a pit-free algorithm, originally developed by Khosravipour et al. (2016), was performed to generate CHMs in the LAStools software. This approach was introduced to avoid empty pixels, and especially pits, from forming, caused by variations in height that would affect further analysis, such as individual tree detection and metrics extraction. This algorithm works by using a subset of point clouds to fill the pits, and has been found to work robustly on high-density and thinned point clouds. It comprises two steps: 1) the construction of a standard CHM and several partial CHMs, each corresponding to the highest part of the canopy; and 2) the combination of these CHMs based on their highest value in each grid cell. In our study, a set of increasing height thresholds, of 2, 5, 10, 15, ..., and 40 m, were used to obtain the partial CHMs. All CHMs were generated using normalized point cloud data that were thinned to half the pixel size instead of all being the first returns. In addition, a ground CHM was included, excluding the normalized point clouds above 0.1 m, in order to fill the potential holes and prevent higher-up canopies from being wrongly connected across water bodies (Isenburg 2014). Finally, the CHMs were merged at a 0.5-m resolution based on the highest value across all CHMs. The pit-free algorithm and the resulting CHM for ALS 2009 acquired in T1 are shown in Figure 4.

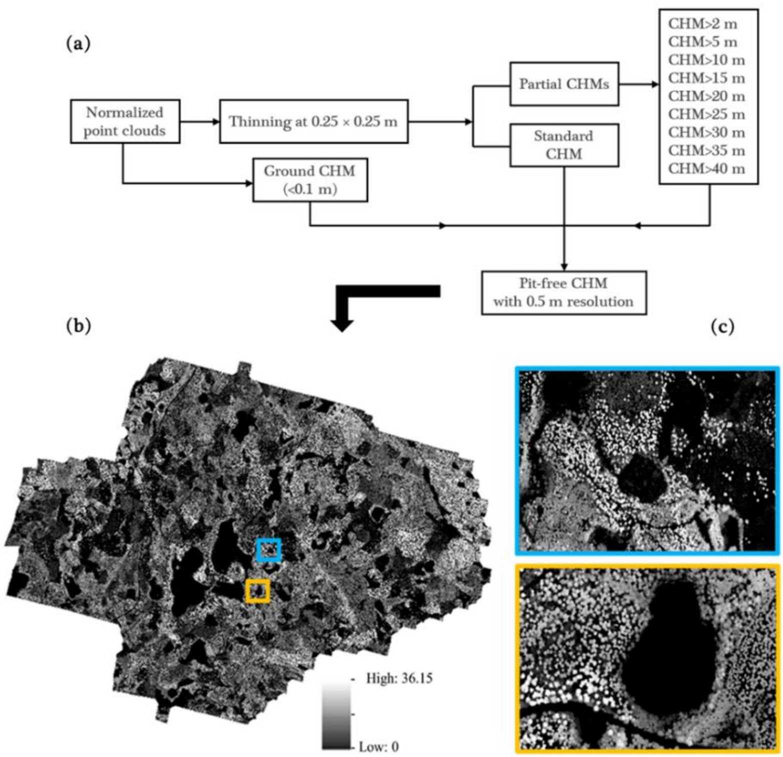

Figure 4. (a) Pit-free algorithm, (b) canopy height model (CHM) of ALS 2009 for the whole study area, and (c) close-up views of (b) (Studies **I** and **III**).

The local maxima filter was applied to identify the treetops on the generated CHMs. Two approaches were applied for the filtering—a fixed window size of 3 × 3 pixels (Studies **I** and **III**) and a variable window size based on an assumed relationship between H and CD, as introduced by Popescu and Wynne (2004) (Study **II**). The identified treetops were then used as markers in the watershed segmentation to delineate crown segments, analogous to pouring water into the inverted CHM. Generated crown segments were used to determine a set of height-normalized points belonging to each tree (or a group of trees with mixed crowns) using a point-in-polygon approach. In Study **II**, however, tree identification was confirmed at the tree stem level, with a Voroni diagram used to split the TLS point clouds if multiple stems were distinguished within a segment.

The individual TLS tree point clouds were divided into stem and crown points based on the method developed by Yrttimaa et al. (2020b) in Study **II**. This classification assumes the stem points have more planar, vertical, and cylindrical characteristics than the points representing the branches and foliage. As a repetitive procedure, starting from the base of a tree (i.e., zero towards the top of the tree), the point clouds were binned into n number of horizontal slices, including P1, P2, …, Pn. The vertical interval of these slices was 4 m for P1 and 50 cm from P2 onward. The idea behind this was to initially access the origin of the stem, which is usually better exposed in the point clouds, while going up the stem requires a more careful exploration due to the presence of foliage. Then, the following procedures were repeated for each slice in order to identify the structural origin of the points and to assign a stem point or crown point classification accordingly. First, to make a uniform point spacing, a grid average downsampling, with a 5-mm grid size, was applied. Second, the surface normal vectors were computed for each point based on their 40-point neighborhood to extract vertical surfaces assumed to represent stems rather than branches. These candidate stem points were further segmented into clusters, with a minimum of 30 cm of Euclidian distance between each, and considering their dimensions. Small and horizontal clusters were neglected, large and vertical clusters were preferred in an attempt to find stem points. Third, a random sample consensus (RANSAC)-cylinder filtering procedure was implemented to remove non-cylindrical structures deviating more than 1.5 cm of Euclidian distance from the surface of the fitted cylinder, with the aim of confirming the cylindrical shape of the candidate stem point clusters. Finally, an alpha shape was created to envelope the candidate stem points and separate them from the crown points. The TLS points falling inside the alpha shape and the TLS and ALS points falling outside the alpha shape were classified as stem and crown points, respectively. The center of the RANSAC cylinder fitted into the stem points at breast height was considered as the tree location.

By applying a height threshold of 2 m (Nilsson 1996), the point clouds of the individual trees belonging to the tree crowns from the airborne datasets were kept and further used for characterizing tree crown structures (Studies **I** and **III**). The location of each tree in the airborne datasets was defined based on the planar location of the highest point in each crown segment. As an example, Figure 5 provides an illustration of the point clouds of an individual tree crown dynamic over time in cross-sectional view (Study **III)**.

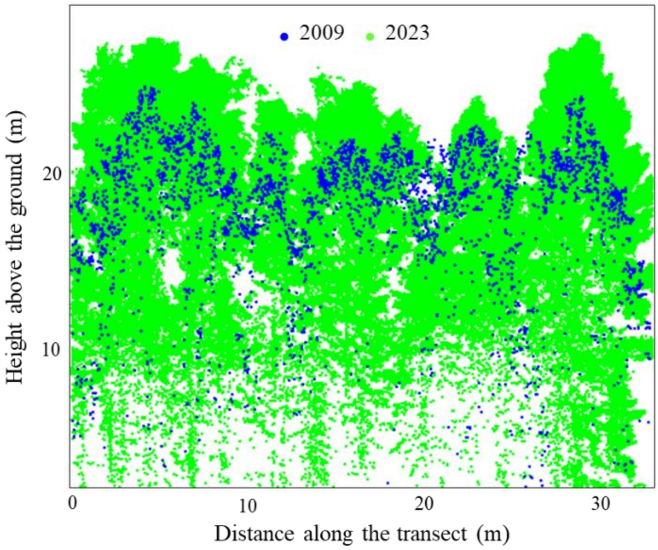

Figure 5. A cross-sectional view of ALS 2009 (T1, blue) and Heli-ALS 2023 (T2, green) point clouds depicting individual trees along a transect (Study **III**).

2.6 Characterizing individual trees into tree and crown metrics

The individual tree stem points derived from TLS 2014 and TLS 2021 were used to compute the stem volume (V) in Study **II.** The procedure developed by Yrttimaa et al. (2019) was utilized to estimate the taper curve, which represents the stem diameter as a function of H. First, the stem points were divided into horizontal slices at 20-cm vertical intervals, starting from 1.30 m above the ground and moving toward the stump and treetop. Then, circles were fitted to those intervals to measure the tree diameters. Outliers in the diameter-height observations were removed following the method in Saarinen et al. (2017). In this method, each diameter is compared with the mean of the three previous diameters and identified as an outlier if the relative difference exceeds 10% for diameters above, and 20% for diameters below, breast height. To level unevenness and interpolate missing values in the diameter-height observations, a cubic spline curve, with a smoothing parameter of 0.5, was fitted. Finally, a taper curve was obtained at 10-cm intervals up to the top of the tree. Considering the stem as a sequence of vertical cylinders in predefined sections at 10-cm height intervals, the Huber formula was used to estimate V based on the estimated taper curve (Equation 1).

$$V = \sum_{i=1}^{n} \frac{\pi h_i}{16} (d_i + d_{i+1})^2 \qquad (1)$$

where h_i and d_i are the height and diameter of cylinder *i*, respectively, and *n* is the total number of cylinders.

To characterize the tree crowns in Study **II**, the individual tree crown points derived from Heli-ALS 2014 and TLS 2014 in T1, and Heli-ALS 2021 and TLS 2021 in T2 were combined. We assumed a higher capability of multisensorial datasets in comprehensively reconstructing tree crown structures. Similarly, in Studies **I** and **III**, the individual tree crown points of the airborne datasets in T1 and T2 were used to characterize the tree crown structures. These datasets included ALS 2009 and ALS 2014 for Study **I** and ALS 2009 and Heli-ALS 2023 for Study **III**.

In Studies **I–III**, the tree crown metrics were determined using geometrical descriptors. A 2D convex hull was applied to calculate the CD and CA. This formed the smallest polygon that could contain all the crown points. The identified points lying on the 2D convex hull were considered for CD calculation, this being the distance between the two outermost crown points in x–y space. The CV and crown surface area (CSA) were computed using a 3D convex hull that encompassed all the crown points within a closed convex made of triangles. In Study **II**, the crown perimeter (CP) was one of the 2D metrics calculated instead of the CD, and the lowest point in the 3D convex hull was considered as the crown base height (CH_{min}). In addition, the CV was computed by voxelizing the points into a 10-cm regular 3D grid, each representing a volume of 1 dm^3. The volume of each voxel containing at least one point was summed to calculate the CV of the individual trees. As a measure of how efficiently a tree utilized resources to achieve a certain architectural structure, the CP/CA and CSA/CV ratios were calculated in Study **II** (Yrttimaa et al. 2022). The H was always determined as the highest point return within the crown segment (Studies **I**–**III**).

2.7 Tree-to-tree matching to calculate increments in the tree and crown metrics

Detecting and analyzing the growth of individual trees over time, and the effect on the wood properties, required links to be established between corresponding point cloud-derived and field-measured trees, known as tree-to-tree matching. In Study **I**, both the tree locations and crown segments were used for the matching processes. Initially, tree species information was obtained by matching T2 ALS 2014 trees to the field-measured trees inventoried in the same year. The crown segment of T2 ALS 2014 was matched with the tallest field tree co-existing within each segment. Next, we overlaid the crown segments of T2 ALS 2014 with the tree locations of T1 ALS 2009, and vice versa. However, the different segmentation accuracy between T1 ALS 2009 and T2 ALS 2014 was observed by the presence of under- and over-segmentation errors. To address this, and ensure proper matching, only those T2 ALS 2014 crown segments that contained a single T1 ALS 2009 tree location were retained, and vice versa. Additionally, we kept the matched trees that existed in both datasets and that did not exhibit a height reduction exceeding 3 m. These heuristic rules accounted for tree mortality, logging, and damage over the 5 years, ensuring that only living trees, which should not have decreased in height, were included. The tree-to-tree matching method was expected to compensate for potential spatial mismatches between tree locations resulting from discrepancies in ALS acquisition and prevailing wind patterns at the time of data collection.

In Study **II**, however, tree-to-tree matching was conducted employing both tree location and similarity in tree metrics. The species information for the T1 trees was obtained by searching for field trees within a distance of 1.5 m. The matched trees were then chosen based on similarity in tree metrics among the possible candidates. Similarly, the trees derived at T1 and T2 were matched to each other. We further concentrated our analysis on those trees that had sufficient point cloud reconstructions at both T1 and T2 by accepting the following threshold for variability between measurements: a difference of less than 3 cm in field and TLS-derived dbh, less than 4 cm in diameter at 6 m height, less than 70% in crown volume, and less than 6 m in H.

A different matching was considered for Study **III**, where we first matched T1 ALS 2009 trees with the closest T2 Heli-ALS 2023 trees within a maximum distance of 2 m. Then, each sample tree with wood properties measured by ITRAX was assigned to the closest respective crown segment left from the first step. This matching rate was also maximized by visual interpretation. These matched trees were used for the tree- and plot-level assessment of wood properties.

The matched trees from Studies **I** and **II** were further divided into three groups by tree species—Scots pine, Norway spruce, and birch. In Study **III**, we considered Scots pine and Norway spruce because we only collected wood samples from these species. An example of species-specific matched trees with their consecutive crown metrics from Study **I** is shown in Figure 6.

To calculate the species-specific increments in the tree (Δ) and crown metrics (ΔC) during the monitoring period, the measurements at T1 were subtracted from the respective measurements at T2. This resulted in ΔV, ΔH, ΔCD, ΔCA, ΔCP, ΔCV, ΔCSA, ΔCH_{min}, Δ(CP/CA), and Δ(CSA/CV). In Study **I**, the relative ΔC (rΔC) was also computed by dividing the ΔC of a specific metric by that metric at T1 in order to minimize the inherent differences in scale between the different trees (Pommerening and Muszta 2015). Each species-specific crown metric having observations three times the inter-quartile larger than the first and third quartile was removed from Study **I**. This was done, in particular, to reduce the probability of a Type II error (Zimmerman 1994) and resulted in sample sizes of 947, 749, and 402 for the Scots pine, Norway spruce, and birch, respectively. A similar approach was considered for removing outliers in Study **II**, but based on growth in stem volume (ΔV), resulting in 219 Scots pine, 112 Norway spruce, and 77 birch trees.

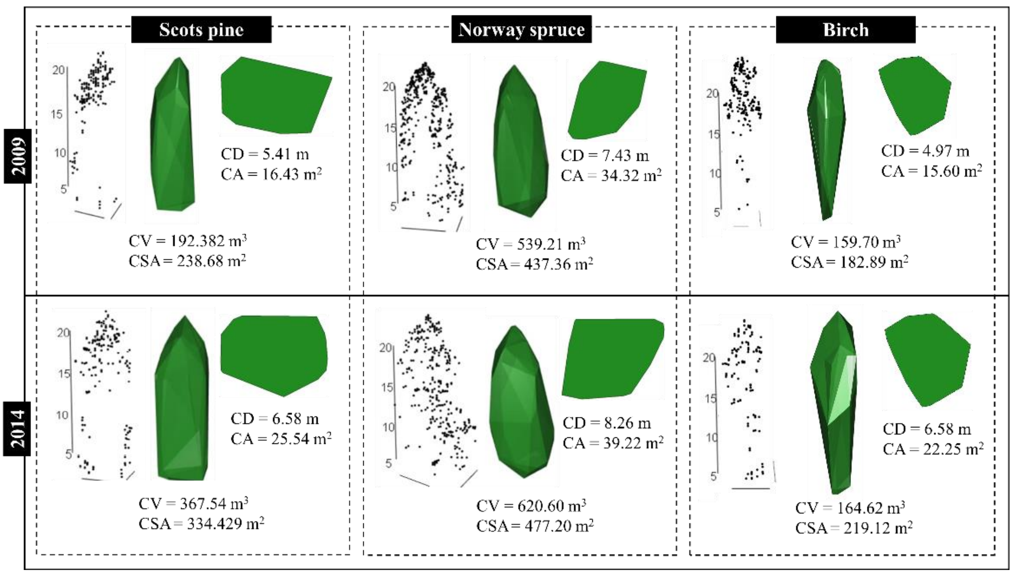

Figure 6. Illustration of the ALS-derived crown metrics in 2009 (T1) and the respective measures in 2014 (T2) for each of the investigated tree species. CD, CA, CV, and CSA are crown width, projection area, volume, and surface area, respectively (Study **I**).

Table 5. Structural characteristics of the matched trees measured in the field plots by tree species in 2014. The mean and standard deviation (Std.) of diameter at breast height (dbh), volume, and height have been reported (Studies **I–III**).

Species	Study	Sample size (n)	Diameter at breast height (cm)		Volume (m^3)		Height (m)	
			Mean	Std.	Mean	Std.	Mean	Std.
Scots pine	I	947	21.74	6.77	0.41	0.36	19.65	4.27
	II	219	19.10	7.77	0.31	0.37	16.75	4.65
	III	257	25.26	7.49	0.58	0.55	20.92	4.61
Norway spruce	I	749	20.42	10.37	0.46	0.50	22.09	5.66
	II	112	21.54	10.02	0.52	0.51	19.74	7.49
	III	142	30.18	8.49	0.96	0.63	25.63	4.49
Birch	I	402	15.73	6.46	0.22	0.24	19.71	4.10
	II	77	16.60	5.63	0.24	0.20	19.18	4.66

In Study **III**, which was based on wood property measurements at an annual resolution, the mean annual increments in H and other crown metrics of individual trees were calculated by dividing the change observed between T1 and T2 by the number of growing seasons between the measurements. Considering two levels of analysis in Study **III**, these tree-level measures were called ΔH_{mean_tree} and ΔC_{mean_tree}, respectively, with a sample size of 257 Scots pines and 142 Norway spruces. To conduct this analysis at the plot level, their means (ΔH_{mean_plot}, ΔC_{mean_plot}) were calculated for 44 and 24 sample plots represented by Scots pines and Norway spruces, respectively. However, to calculate the plot-level standard deviations (ΔH_{std_plot}, ΔC_{std_plot}), only sample plots with at least three observations per species were considered, leaving 38 sample plots for Scots pine and 21 sample plots for Norway spruce. The field-measured structural characteristics for the final sets of trees used in the analysis are provided in Table 5.

2.8 Statistical analysis and accuracy assessment

For Study **I**, a paired-sample *t*-test was employed to evaluate the statistical significance of species-specific differences in the means of the crown metrics measured at the beginning and end of the 5-year monitoring period (within-group comparison). Considering the skewed distributions of CA, CV, and CSA and the potential deviation from normality, the Wilcoxon signed-rank test was also conducted in order to compare within-group species-specific differences in the crown metric medians. Although we can assume that the sample means came from a normal distribution, this does not guarantee the normal distribution of the population (Kim and Park 2019). The rstatic package of R (Kassambara 2023) was used for this task, and the results are reported at a 95% confidence interval. To evaluate statistical differences in the means/medians of the rΔCD, rΔCA, rΔCV, and rΔCSA between-species groups (between-groups comparison), a Welch analysis of variance/Kruskal–Wallis test was performed due to violation of the variance homogeneity and non-normal distribution. This was followed by paired-sample *t*-test and Wilcoxon test comparisons of the between-species groups. We applied the Bonferroni correction to control the probability of committing a Type I error. Thus, the *p* values were divided by the number of comparisons (Triola et al. 2006).

The effect size was also measured, using Cohen's D and the generalized eta squared (η^2) in Study **I** (Cohen 2013; Olejnik and Algina 2003). These helped us to understand the strength of the difference in this study. Cohen's D quantifies the size of the difference between the means of two groups using their standard deviation. Contrastingly, η^2 was used to explain the variability caused by the different groups, while minimizing the dependency on the research design. To interpret the results, the following rules of thumb were used: Cohen's D values of 0.2, 0.5, and 0.8, and η^2 values of 0.01, 0.06, and 0.14 denote a small, medium, and large effect size, respectively.

In Studies **I** and **II**, the consistency of the tree and crown metrics derived from the bi-temporal point clouds at T1 and T2 were assessed using Pearson's *r* and the visual inspection of scatterplots. Consistency was achieved if the measurements were not significantly influenced by random measurement error, the observed variations then instead reflecting a real change. Employing *r*, the linear relationships between ΔV and the crown metrics in T1 were assessed, as well as their ΔC, in Study **I**. This was also used in Study **III**, in assessing the relationship between WD_{mean_tree} and RW_{mean_tree} with ΔH_{mean_tree} and ΔC_{mean_tree}, as well as their respective plot-level measures of means and standard deviations. These analyses were applied across different tree species and a 95% confidence interval was used.

In additon, a random forest (RF) regression was used to explain these species-specific relationships in Study **II**, allowing us to assess the potential nonlinearity in these relationships. Also, RF is well-suited to address interaction effects due to its ensemble structure, which combines multiple decision trees to achieve more-accurate predictions (Breiman 2001). Despite its capacity to somewhat handle collinearity, we retained the highest-correlating metrics and eliminated their most redundant counterparts ($r > 0.8$). In addition, the relative importance of selected predictors was computed using the Gini index and scaled into a range of 0–100. This quantified the extent to which the metrics contributed to reducing the impurity of the decision tree nodes (Hapfelmeier et al. 2014). In Study **III**, instead, a multiple linear mixed-effect regression, accounting for the variability caused by the different sample plots, was used for assessing species-specific wood properties at the individual tree level (Equation 2). The LME4 package in R software was used for this purpose (Bates et al. 2015).

$$y_{ij} = \beta_0 + \beta_1 x_{1ij} + \beta_2 x_{2ij} + \cdots \beta_n x_{nij} + b_{0i} + \varepsilon_{ij} \tag{2}$$

where y_{ij} is the response variable of interest (i.e., WD_{mean_tree} or RW_{mean_tree}) for tree j within sample plot i, x_{1ij},…,x_{nij} represent the fixed effects variables, β_0, β_1,…,β_n are the corresponding coefficients, b_{0i} and ε_{ij} denote a normally distributed random effect for plot i and the residual error, respectively, with a mean zero and an unknown, unrestricted variance–covariance matrix. The fixed effects were all also scaled into a range of 0–1, using the min–max method to compare their contribution to the model. The formula is $f(x) = (x_i – x_{min})/(x_{max} – x_{min})$, where x_i stands for the fixed effect variable of interest for tree *i*, and x_{min} and x_{max} are its minimum and maximum values across all trees, respectively. It is worth mentioning that the best model was selected based on the balance between the model fit and its complexity, as measured by the Akaike information criterion. For this purpose, models with different combinations of predictors were developed utilizing the MuMIn package in R (Barton 2015). At the plot level, multiple linear regression was applied to the WD_{mean_plot} and RW_{mean_plot} models, employing the Stats package in R (R Core Team 2021). A similar systematic approach to linear mixed-effect regression was conducted to find the best combination of predictors based on the Akaike information criterion.

To quantify the proportion of observed variation in the variable of interest that could be explained by the above-mentioned metrics, R^2 was used in Study **II** and the plot-level models of Study **III**. However, the proportion of variance explained by fixed effects and both fixed and random effects was separately explained by marginal R^2 (R^2_m) and conditional R^2 (R^2_c) values in the individual tree-level models of Study **III**, respectively.

3 RESULTS

3.1 Feasibility of bi-temporal ALS data in detecting increments in crown metrics (Studies I and II)

The results of the paired *t*-test in Study **I** revealed a statistically significant ($p < 0.0001$) difference across all species in the mean values of the ALS-derived CD, CA, CV, and CSA between T1 and T2, indicating a change in the examined metrics. Within a 5-year time interval, the estimated ΔCD ranged from 0.30 to 0.56 m, with corresponding Cohen's D values ranging from 0.32 to 0.62 across all species. A maximum ΔCA was found for Scots pine (3.57 m^2) and indicated a large size of effect (Cohen's D = 0.93). The estimated ΔCA also differed by 0.75 and 0.42 standard deviations for Norway spruce and birch, respectively. Cohen's D was the highest for ΔCV, ranging from 1.09 to 1.22, and ΔCSA, ranging from 1.26 to 1.46. The observed ΔCV was 86.30 m^3 for Norway spruce, 62.86 m^3 for birch, and 61.90 m^3 for Scots pine. Meanwhile, the ΔCSA varied from 51.73 to 60.44 m^2 across all species. The results of the Wilcoxon signed-rank test also showed a statistically significant difference in the median values of the crown metrics between T1 and T2.

A further exploration of the variability of the point cloud-based stem and crown measurements between tree individuals was depicted in scatter plots representing the T1 versus T2 measurements. Figure 7 shows an example from Study **II** where the relationship between the stem and crown metrics is shown and measured by the correlation coefficients. The H and V are shown as the most consistent measurements over time, with $r > 0.97$, regardless of tree species. The CV also showed the greatest agreement between the T1 and T2 measurements for Scots pine ($r = 0.85$), followed by Norway spruce ($r = 0.82$) and birches ($r = 0.74$). In general, rather consistent measurements were achieved for CA, CSA, CP, and CP/CA as well, although the observations were more scattered around the 1:1 line. The lowest correlations were obtained for CSA/CV ($r = 0.4$–0.65), followed by CH_{min} ($r = 0.58$–0.7), indicating moderate consistency and thus less reliable measurements over time. Similar results were obtained in Study **I**, where the crown metrics of all the tree species showed consistency over the 5-year time interval ($r = 0.70$–0.94).

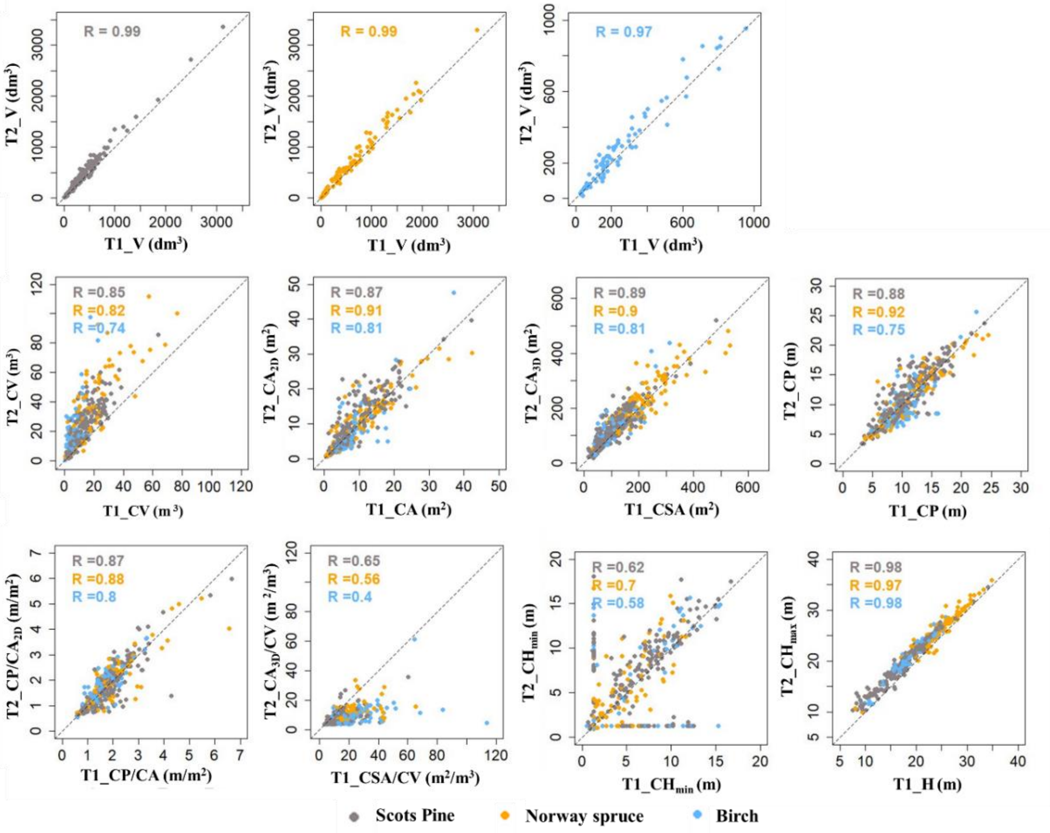

Figure 7. Scatter plots and Pearson's correlation coefficient (*r*) visualize the consistency of species-specific individual tree and crown metrics measured using T1 Heli-ALS (2014) and T2 Heli-ALS (2021). These metrics include tree stem volume (V) and height (H), as well as the crown metrics of volume (CV), 2D projection area (CA), surface area (CSA), perimeter (CP), perimeter to projection area ratio (CP/CA), surface area to volume ratio (CSA/CV), and base height (CH_{min}) (Study **II**).

In addition, the results of the Welch analysis of variance, as implemented in Study **I**, demonstrated that the means of rΔC varied significantly among the species groups, with *p*-value < 0.0001 (Table 6). The pairwise *t*-test comparisons revealed a statistically significant difference in rΔCD between Scots pine and birch, as well as between Scots pine and Norway spruce (*p*-value < 0.0001). However, there was no significant difference in the rΔCD between Norway spruce and birch (Figure 8).

Table 6. Species-specific relative increments in the crown metrics (rΔC) derived from ALS 2009 (T1) and 2014 (T2). These metrics include width (CD), projection area (CA), volume (CV), and surface area (CSA). Mean, standard deviation (Std.), *p*-value, and generalized eta squared effect size (η2) have been reported (Study **I**).

Metric	Species group	rΔC (%)		*P-value*	η^2
		Mean	Std.		
CD	Scots pine	15.38	23.30	2.18e-8	0.02
	Norway spruce	10.50	18.50		
	Birch	8.54	20.89		
CA	Scots pine	35.42	41.05	2.4e-22	0.05
	Norway spruce	21.96	26.98		
	Birch	15.64	32.16		
CV	Scots pine	97.67	94.77	1.93e-16	0.03
	Norway spruce	58.21	48.32		
	Birch	74.97	96.86		
CSA	Scots pine	55.80	53.48	1.73e-19	0.04
	Norway spruce	34.14	27.24		
	Birch	46.89	58.91		

Using the Kruskal–Wallis test, a statistically significant difference was found, in Study **I**, among species groups for the medians of rΔCA, rΔCV, and rΔCSA (Table 6). The pairwise Wilcoxon test indicated significant differences in the median values of rΔCV and rΔCSA between Scots pine and Norway spruce and between Scots pine and birch (Figure 8). However, there was no significant difference in rΔCV and rΔCSA between Norway spruce and birch. Unlike rΔCD, rΔCA showed a significant difference between Norway spruce and birch (*p*-value < 0.0001). On average, the rΔCD, rΔCA, rΔV, and rΔCSA of Norway spruce showed lower standard deviations compared to the other species, ranging from 18.50 to 48.32%. The highest variability was observed in the rΔCSA and rΔCV of birch (Std. of 58.91 to 96.86%) and in the rΔCD and rΔCA of Scots pine (Std. of 23.30 to 41.05%) (Table 6). The η^2 values were moderate for rΔCA (0.05), and lower for rΔCSA (0.04), rΔCV (0.03), and rΔCD (0.02) (Table 6).

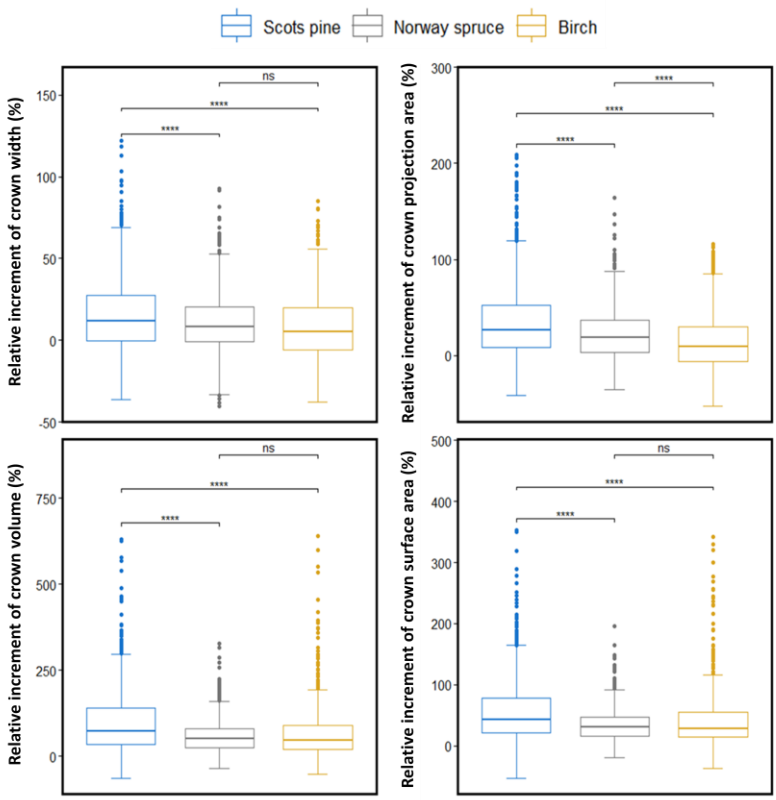

Figure 8. Pairwise comparisons of relative crown increments (rΔC) between different species groups. **** and ns (not significant) denote p-value < 0.0001 and > 0.05, respectively (Study **I**).

3.2 The relationship between stem volume growth and crown metrics, including their increments characterized by multisensorial point clouds (Study II)

Table 7 presents the relationships between various crown metrics, including their increments and the ΔV for Scots pine, Norway spruce, and birch, as analyzed in Study **II**. For Scots pine, H, CA, and CP showed the strongest positive correlations with ΔV (r = 0.61–0.62, p-values < 0.05), with CSA, CV, and ΔCV also having significant positive correlations (r = 0.52-0.54, p-values < 0.001), while CP/CA had a negative correlation with ΔV (r = –0.46). For Norway spruce, CSA, ΔCV, CV, and CP had the highest correlations with ΔV (r = 0.37–0.38), followed by CA and H (r = 0.34–0.35). The birch ΔV was most strongly correlated with ΔCV (r = 0.45, p-values < 0.001), with CP and CA showing weaker correlations (r = 0.38 and 0.39, respectively).

Table 7. Species-specific Pearson's correlation coefficients measuring the relationships between stem volume growth (ΔV) and tree height (H) and its increment (ΔH) as well as other crown metrics and their increments (ΔC): 2D projection area (CA), perimeter (CP), volume (CV), surface area (CSA), perimeter to projection area ratio (CP/CA), surface area to volume ratio (CSA/CV), and base height (CH_{min}). These metrics were calculated using ALS 2014 (T1) and HeliALS-2021 (T2). Significance level denoted as ^{ns} (not significant) for *p*-value > 0.05, * for *p*-value < 0.05, ** for *p*-value < 0.01, and *** for *p*-value < 0.001. Metrics sharing the same superscript letter represent collinear pairs with a correlation coefficient (*r*) exceeding 0.8 (Study **II**).

Species/Tree and crown metrics	Scots pine (n = 219)		Norway spruce (n = 112)		Birch (n = 77)	
	ΔV					
	Cor	*p*-value	Cor	*p*-value	Cor	*p*-value
CA	0.61^{ac}	$< 0.001^{***}$	0.35^{ade}	$< 0.001^{***}$	0.39^{a}	$< 0.001^{***}$
CP	0.61^{bcd}	$< 0.001^{***}$	0.37^{cef}	$< 0.001^{***}$	0.38^{ab}	$< 0.001^{***}$
CV	0.52^{ab}	$< 0.001^{***}$	0.37^{abc}	$< 0.001^{***}$	0.27	0.016^{*}
CSA	0.54	$< 0.001^{***}$	0.38^{bdf}	$< 0.001^{***}$	0.31	0.006^{**}
CP/CA	-0.46^{d}	$< 0.001^{***}$	–0.27	0.004^{**}	-0.29^{b}	0.010^{*}
CSA/CV	–0.23	$< 0.001^{***}$	-0.30^{g}	0.001^{**}	-0.15^{c}	0.183^{ns}
CH_{min}	0.41	$< 0.001^{***}$	0.31	$< 0.001^{***}$	0.09	0.456^{ns}
H	0.62	$< 0.001^{***}$	0.34	$< 0.001^{***}$	0.27	0.015^{*}
ΔCA	0.20^{e}	0.002^{**}	0.21^{h}	0.026^{*}	0.18^{d}	0.111^{ns}
ΔCP	0.13^{e}	0.045^{*}	0.20^{h}	0.030^{*}	0.20^{de}	0.073^{ns}
ΔCV	0.52	$< 0.001^{***}$	0.38	$< 0.001^{***}$	0.45	$< 0.001^{***}$
ΔCSA	0.15	0.021^{*}	–0.05	0.611^{ns}	0.08	0.500^{ns}
Δ(CP/CA)	–0.12	0.066^{ns}	–0.13	0.169^{ns}	-0.09^{e}	0.451^{ns}
Δ(CSA/CV)	0.04	0.588^{ns}	0.15^{g}	0.107^{ns}	0.07^{c}	0.557^{ns}
ΔCH_{min}	0.10^{f}	0.154^{ns}	0.17^{i}	0.075^{ns}	0.24^{f}	0.035^{*}
ΔH	0.10^{f}	0.124^{ns}	0.18^{i}	0.056^{ns}	0.24^{f}	0.038^{*}

In addition, three RF models were developed to explain the ΔV of the Scots pine, Norway spruce, and birch trees (Study **II**). Figure 9 shows the importance of predictor variables in the mentioned models, based on the scaled mean decrease in the Gini index. The most important metric for explaining the Scots pine ΔV was H, followed by CP and CP/CA, with relative importance values of 45.09 and 44.19, respectively (Figure 9). For Norway spruce, ΔCV had the highest relative importance in explaining ΔV, while it was 86.46 for CV, 77.28 for ΔCSA, and 65.21 for H. For birches, ΔCV was identified as the most important predictor, with CP and CSA emerging as the second- and third-ranked metrics in explaining the birch ΔV, with relative importance values of 90.44 and 80.17, respectively. The substantial impact on the birch ΔV was also found for its CV (75.95), ΔCP (70.07), and H (69.52) (Figure 9). Using these metrics, the model explained 50% of the variation in the Scots pine ΔV (R^2 = 0.50). By contrast, only 20 and 6% of the variation in the ΔV of Norway spruce and birch trees, respectively, were explained by the models incorporating crown metrics and their changes.

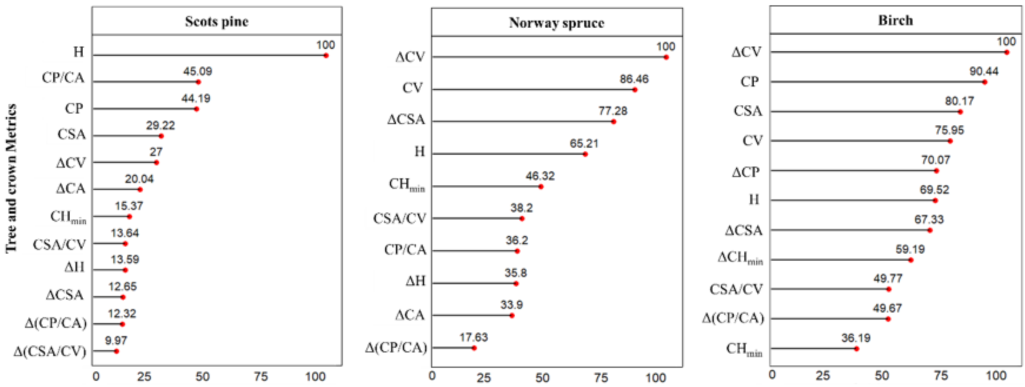

Figure 9. Relative importance of tree and crown metrics in determining stem volume growth (ΔV) for Scots pine, Norway spruce, and birches. These metrics include tree height (H), crown metrics of projection area (CA), perimeter (CP), volume (CV), surface area (CSA), perimeter to projection area ratio (CP/CA), surface area to volume ratio (CSA/CV), and base height (CH$_{min}$), as well as their increments—ΔH and ΔC (Study **II**).

3.3 The relationship between wood properties and ALS-derived increments in crown metrics (Study III)

At both the tree and plot levels, the increased mean annual increment in H (i.e., ΔH_{mean_tree} and ΔH_{mean_plot}) was significantly associated with increased RW_{mean_tree} and RW_{mean_plot} (p-value < 0.001). This association was r = 0.43–0.44 at the tree level and r = 0.47–0.48 at the plot level, regardless of species. Additionally, ΔCA_{mean_tree}, ΔCV_{mean_tree}, and ΔCSA_{mean_tree} were among the correlated metrics with Scots pine RW_{mean_tree}, with correlations of 0.21, 0.17, and 0.16, respectively.

In terms of WD_{mean_tree}, ΔH_{mean_tree} was the only metric with a low, but significant, correlation to WD_{mean_tree} in Norway spruce (r = –0.17 and p-value < 0.05). However, we did not find any significant correlations between WD_{mean_tree} and the studied metrics in Scots pine (p-value > 0.05). At the plot-level, instead, a correlation of 0.36 was observed between the WD_{mean_plot} and ΔCSA_{mean_plot} of Scots pine, whereas no metrics were significant in relation to WD_{mean_plot} in Norway spruce (p-value > 0.05).
When assessing the standard deviations of wood properties at the plot level, neither ΔH_{std_plot} nor ΔC_{std_plot} showed any significant correlation with RW_{std_plot} or WD_{std_plot} in both species (p-value > 0.05).

The models used for assessing wood properties in Study **III** are summarized in Table 8. The ΔH_{mean_tree}, along with the ΔCV_{mean_tree} and ΔCSA_{mean_tree}, significantly contributed to the Scots pine RW_{mean_tree}, with coefficient estimates of 2.39, –1.57, and 0.99, respectively (Table 8). This means an increase in ΔH_{mean_tree} and ΔCSA_{mean_tree} led to an increase in RW_{mean_tree}, while a higher ΔCV_{mean_tree} was associated with a decrease in RW_{mean_tree} (R^2_m = 0.20). For Norway spruce, ΔH_{mean_tree} was the only metric affecting RW_{mean_tree}, with a coefficient estimate of 1.20 and a standard error of 0.27, suggesting that an increase in ΔH_{mean_tree} will increase the RW_{mean_tree} (R^2_m = 0.16). Utilizing these metrics and sample plots as a random effect, 40–41% of the variations in RW_{mean_tree} were explained, regardless of species.

For the WD_{mean_tree} of Scots pine, both ΔCV_{mean_tree} and ΔCSA_{mean_tree} significantly contributed to the model. Their coefficient estimates were –0.18 and 0.15, explaining 4% of the variation ($R^2_m = 0.04$). However, the inclusion of variability between sample plots slightly improved the model performance ($R^2_c = 0.14$). None of the metrics were statistically significant in explaining the Norway spruce WD_{mean_tree} (Table 8). At the plot level, the WD_{mean_plot} model of Scots pine included ΔCSA_{mean_plot} as the only significant predictor, with a low coefficient estimate of 0.06 ($R^2 = 0.11$) (Table 8). In addition, none of the studied metrics were statistically significant in explaining the WD_{mean_plot} of Norway spruce. For RW_{mean_plot}, however, ΔH_{mean_plot} was significantly incorporated into the Scots pine and Norway spruce models, explaining 21 and 18% of the observed variations, respectively. The coefficient estimates of ΔH_{mean_plot} were 0.73 (p-value < 0.001) for Scots pine and 0.71 (p-value < 0.05) for Norway spruces (Table 8). This indicates that, as the change in ΔH_{mean_plot} increases, the RW_{mean_plot} also tends to increase.

Table 8. The coefficient estimates (CE), standard errors (SE), and *p*-values for the models predicting basal area weighted mean wood density and mean ring width using ALS 2009 (T1) and HeliALS 2023 (T2) at the levels of the individual tree (WD_{mean_tree}, RW_{mean_tree}) and plot (WD_{mean_plot}, RW_{mean_plot}). The level of significance is denoted as ^{ns} (not significant) for *p-values* > 0.05, * for *p*-value < 0.05, ** for *p*-value < 0.01, and *** for *p*-value < 0.001 (Study **III**).

Model parameters			CE	SE	*p*-value	CE	SE	*p*-value
			WD_{mean_tree}			**RW_{mean_tree}**		
Tree level	Scots pine (n = 257)	Intercept	0.55	0.01	2e-16***	0.42	0.13	0.002**
		ΔCV_{mean_tree}	–0.18	0.06	0.003**	2.39	0.57	<0.001***
		ΔCSA_{mean_tree}	0.15	0.05	0.003**	–1.57	0.49	0.002**
		ΔH_{mean_tree}	—	—	—	0.99	0.17	<0.001***
	Norway spruce (n = 142)	Intercept	0.46	0.01	2e-16***	0.77	0.12	<0.001***
		ΔH_{mean_tree}	—	—	—	1.20	0.27	<0.001***
			WD_{mean_plot}			**RW_{mean_plot}**		
Plot level	Scots pine (n = 44)	Intercept	0.50	0.01	2e-16***	0.90	0.11	3.58e-10***
		ΔH_{mean_plot}	—	—	—	0.73	0.20	<0.001***
		ΔCSA_{mean_plot}	0.06	0.02	0.01*	—	—	—
	Norway spruce (n = 24)	Intercept	0.46	0.01	2e-16***	1.02	0.11	8.56e-09***
		ΔH_{mean_plot}	—	—	—	0.71	0.28	0.02*

4 DISCUSSION

4.1 Feasibility of point clouds in the detection of increments in crown metrics as well as species-specific differences

The experiments carried out in Study **I** showed that it was possible to used bi-temporal ALS data to detect increments in CD, CA, CV, and CSA over a 5-year monitoring period, providing empirical evidence to answer the set research question (**RQ1**). We observed an overall growth trend for all the investigated crown metrics and, based on statistical tests, the observed trend was unlikely to be due to chance (p-value < 0.0001). This finding acknowledges that while there may be some degree of error or variability in the consequent measurements, the observed growth trend can be considered strong enough to exceed what would be expected from random chance alone. The most prominent change was observed in the ΔCSA of Norway spruce, followed by Scots pine, and birch. A similar pattern was found for ΔCV, indicating large to very large size effects, which is in line with the findings of Frew et al. (2016). They examined the capability of ALS to detect an increase in CV across Douglas fir trees based on field measurements. This included an overall assessment of 220 sample trees, manually segmented over four growing seasons. They found no difference between the predicted CV growth in the field and the corresponding CV growth derived from the ALS data at a 95% confidence interval. The characterization of crown metrics, particularly CV and CSA, was also consistently repeated over time using ALS, as per the findings obtained in Study **I**. Similar results were also obtained in Study **II**, regarding the capacity of the combined point clouds of TLS and low-altitude ALS, where H, V, and CV represented the most consistent measurements over time. This overall consistency was also achieved for other crown metrics, despite the observed variation, which could be attributed to the plasticity of the crown over time and/or potential measurement errors (Figure 7). This is in line with the results of Ma et al. (2018), in which the increments in tree H, CA, and CV of 114,000 trees in conifer-dominated forests were assessed using bi-temporal ALS data. Tree crowns delineated by marker-controlled watershed algorithms showed overall increments in the studied metrics over a 5-year time interval. However, the presence of negative values and high standard deviations also indicated a disparity in the crown metrics. Duncanson and Dubayah (2018) determined a limited feasibility of bi-temporal ALS in monitoring the growth of tree H, crown radius, and CA over 5 years. Their study was conducted over 12 sample plots in California, consisting of mature forests. A modified watershed algorithm was also implemented for crown segmentation to identify both over- and understory trees. The results showed a preserved pattern between the T1 and T2 measures, but a systematic negative bias was observed in the T2 measures of crown radius and CA in the histograms, acknowledging the effect of disparities between the ALS acquisitions. The H estimates appeared to be generally unbiased, however.

A significant difference was also found in the growth patterns of Scots pine, Norway spruce, and birch trees, as assessed by relative increments in the crown metrics (rΔC) (**RQ2**). Study **I** showed that Scots pine featured higher rΔCD, rΔCA, rΔCV, and rΔCSA values during the 5-year time interval compared to Norway spruce and birches, highlighting significant differences between the species (Figure 8). Contrastingly, birch differed from Norway spruce only in terms of the magnitude of the rΔCA recorded during the monitoring period. As shown in Table 5, birches as pioneer tree species prioritize H growth over dbh, reaching the canopy to compete for light and maximize their photosynthesis efficiency. Our findings align with this, with more relative growth in the CV and CSA of birches than in the CD and CA (Table 6). Generally, coniferous trees are among the least flexible in their crown development, with a low ability to close gaps (Getzin and Wiegand 2007), although our experiments did not provide statistical evidence for the rΔCD being different between birch and Norway spruce, which partially corresponds with the results obtained by Vepakomma et al. (2011) (Figure 8). However, only 2–5% percent of rΔC variations can be explained by tree species. This finding can be attributed to the highest variability of rΔC within each species group, with the highest variability recorded for CV, followed by CSA. This means other biotic factors, such as tree size or age, stem density, and competition, as well as abiotic factors, such as the soil nutrient level, local climate, topography, and water balance, are likely to have more control over the growth process (Aakala et al. 2013; Kaitaniemi and Lintunen 2010; Rapp et al. 2012; Stephenson et al. 2014; Weiskittel et al. 2011). In addition, the reliable characterization of structural changes in trees using ALS largely depends on the accuracy of detecting the trees, correctly delineating them from the point clouds, and accurately estimating their metrics. The ALS point density is an important factor that affects raster-based tree detection methods, as applied in this work. According to Zhao et al. (2018), growth analysis at the tree level required densities of at least 7 points/m^2, which was almost met in our studies, based on the ALS data. However, the rate and accuracy of detection are higher for dominant and co-dominant trees than for intermediate and suppressed trees (Jakubowski et al. 2013; Vastaranta et al. 2011). This leads to a bias in plot-level analysis because of erroneous parameter estimations or the omission of intermediate and suppressed trees, especially in complex forests (Tompalski et al. 2021; Yu et al. 2004).

4.2 Explaining species-specific stem volume growth

In Study **II**, crown metrics and their increments, derived from multisensorial point clouds, demonstrated varying relationships in explaining the ΔV across different tree species (**RQ3**). The H, CP, and CA were strongly correlated with the Scots pine ΔV, with CP and CA moderately related to the ΔV of birches (Table 7). The most dominant role of H was in predicting the ΔV in Scots pine, as obtained by RF, but with relatively lower impacts for Norway spruce and birches (Figure 9). This suggests that taller trees may have had a competitive advantage over smaller trees, leading to the increased ΔV. In particular, the strong effect of H in explaining the variation in the ΔV of Scots pine underlines its higher demand for light compared to Norway spruce (Givnish 1988). Additionally, CP was found to be a more significant predictor for Scots pine and birch compared to a late-successional Norway spruce (Figure 9). An increase in CP can secure access to light by providing greater leaf area for photosynthesis, ultimately leading to stem volume growth (Poorter et al., 2012). A similar study was conducted by Pretzsch (2021), who used an experimental setup, consisting of 1,596 trees, including Norway spruce, Scots pine, European beech (*Fagus sylvatica* L.), and sessile oak (*Quercus petraea* [Matt.] Liebl.). The results showed the effects of internal, structural, and morphological characteristics on predicting the stem volume growth that reduced the RMSE by 43% compared with the baseline model, with stem volume as a predictor (RMSE = 0.67 m^3/year). Consistent with our findings, there was a strong positive effect related to the CA, with coefficient estimates of 0.21. However, these relationships are complex and might also be caused by other drivers, such as stand density.

As discussed in Valentine et al. (2012), H is highly affected by stand density, and constrained crown sizes due to high stand density could affect the overall growth rate of trees.

The Norway spruce ΔV was moderately correlated with the metrics representing the 3D structure of the crown, including CSA, CV, and ΔCV (Table 7). Similarly, ΔCV, CV, and ΔCSA also showed high relative importance in assessing the combined effects of crown metrics. This is in line with the Norway spruce's preference to effectively capture light throughout expanding its crown as a shade tolerance species (Givnish 1988). A theoretical approach to how stem mass density at crown base height can affect the growth of an entire tree has been presented by Osawa et al. (1991). This is the so-called profile theory of tree growth, and it has shown promising results in predicting tree growth in different species by incorporating height growth, foliage mass, and length of clear bole into the model. In our study, the CH_{min} of Norway spruce also showed a significant relationship with ΔV—both individually, as well as in combination with other metrics. This finding is consistent with that of Yrttimaa et al. (2022), who utilized TLS in a boreal forest. They found the strongest correlation in Norway spruce, with an R^2 of 0.59, linking the CH_{min} to growth in the volume of the stem section below the height corresponding to 50% of the H. However, the observed variation in CH_{min} might influence these relationships (Figure 7). This is likely associated with measurement errors, such as inaccuracy in the classification of points into stem and crown categories, the presence of neighbors in the tree's branch architecture, and imputed values for the trees for which CH_{min} could not be directly calculated. Notably, CH_{min} was not a highly-ranked metric for explaining the Scots pine ΔV in our study (Figure 8). However, previous research has shown that variation in CH_{min} driven by stand density can affect stem growth (Beekhuis 1965; Fish et al. 2006; Mäkelä and Valentine 2006).

As can be seen, the crown metrics measured in T1 had a stronger linear correlation with ΔV across all species, aligning with the findings presented by Yrttimaa et al. (2022) (Table 7). This implies that trees with initially larger crowns are more likely to exhibit an increased ΔV compared to those with smaller crowns, suggesting a weaker competitive status. However, the ΔCV and ΔCSA in Norway spruce trees and the ΔCV, ΔCP, and ΔCSA in birch trees were found to be influential metrics for describing ΔV using RF (Figure 9). This suggests that Norway spruce and birch continue to develop their crowns to maintain their growth rates. Overall, Scots pine had the strongest relationship between H and other crown metrics and their increments with ΔV, followed by Norway spruce and birches, as indicated by the higher R^2 values. However, it should be mentioned that the smaller sample size and the leaf-off season during data acquisition likely contributed to the lowest R^2 recorded for birch trees. It is also important to note that the relationships presented here might have been influenced by various factors, including site conditions, provenance, and tree age (Pretzsch et al. 2022). Therefore, generalizing these findings requires their further exploration. Additionally, while this study focused on crown characteristics, it is essential to acknowledge that tree growth is a complex process, influenced by a combination of factors, including internal tree and stem characteristics, as demonstrated by Pretzsch (Pretzsch 2021). In this study, we assumed the potential capabilities of multisensorial point clouds to improve occlusion within a crown segment, and the segmentation was also optimized for cases where multiple trees were identified within a segment. However, the correctness of crown segmentation, extraction of tree and crown metrics, and their consistency over time may still be limited. The errors related to the co-registration accuracy between Heli-ALS and TLS may also have resulted in a mismatch between the trees identified at T1 and T2, thus reducing the number of trees that were correctly linked to the field-measured trees. Another source of uncertainty is that, in a slow-growth boreal forest, detecting change with a magnitude that falls within the accuracy limits of the measurement technique can be problematic (Luoma et al. 2021; Yu et al. 2004). For instance, the presence of negative ΔV observations in this study, most likely attributed to point cloud occlusion and inaccurate taper curve estimation, has caused uncertainty in the analysis and interpretation of the relationships. Accordingly, understanding the time interval to overcome excess noise and reveal real patterns can be crucial in forest change detection (Coops 2015; Socha et al. 2017a; Yu et al. 2004).

4.3 Assessing wood properties and their variations

In Study **III**, we demonstrated the link between ALS-derived mean annual increments in H and crown metrics over 15 growing seasons to the wood properties of individual trees or sample plots (**RQ4**). When assessing the relationship at the tree level, a significant correlation was observed between the Scots pine RW_{mean_tree} and its ΔH_{mean_tree}, along with all the other crown metrics. Notably, ΔH_{mean_tree} was also the only metric that significantly correlated with the RW_{mean_tree} of Norway spruce in our experiment. This association was also observed at the plot level between the ΔH_{mean_plot} and RW_{mean_plot} of both Scots pine and Norway spruce. The results from modeling RW also revealed the importance of H increment as a significant predictor at the tree and plot levels for both tree species (Table 8). Accordingly, increased H directly impacts the tree's radial growth, as reflected in the width of the growth rings. This is in agreement with previous findings that showed the effect of height growth on radial growth, modulated by stand density, such as Valentine et al. (2012). By contrast, Kankare et al. (2022) found no significant correlation between increment in H, obtained from the difference between TLS-derived and field-measured height, and the past mean RW of trees. This difference might be attributable to the enhanced capability of ALS in accurate height estimation due to its above-canopy viewpoint (Wang et al. 2019). This also suggests a more complex interplay between tree H increment and mean RW over a longer time scale than the applied 15 growing seasons, which is still considered a rather short period considering the lifespan of boreal trees. In addition to ΔH_{mean_tree}, we observed significant correlations between the other crown metrics and the RW_{mean_tree} of Scots pine at the tree level. In particular, ΔCSA_{mean_tree} and ΔCV_{mean_tree}, included in the Scots pine RW_{mean_tree} model, imply an interplay between photosynthetic leaves and growth rate (Pretzsch et al. 2022). ΔH_{mean_tree}, however, was the only significant predictor in the RW_{mean_tree} model of Norway spruce (Table 8), whereas a recent study conducted by Ahmed et al. (2024) reported correlations of 0.73 and 0.54 when investigating the mean RW of 122 Norway spruce trees in relation to their crown radius and tree H, respectively. They employed single time-point TLS using an intensive scan setup with manual tree segmentation and dendrochronological RW patterns under diverse growing conditions. Similarly, Pretzsch et al. (2022) explained variation in the annual diameter growth of Norway spruces using a TLS-derived standard deviation in the maximum crown radius along the stem axis, and crown top-heaviness.

In terms of WD_{mean_tree}, neither ΔH_{mean_tree} nor ΔC_{mean_tree} were significantly correlated with the WD_{mean_tree} of Scots pine. However, ΔCSA_{mean_tree} and ΔCV_{mean_tree} were included in the model as significant predictors for Scots pine. Our findings were consistent with those of Kankare et al. (2022), who used single time-point TLS with automatic segmentation to study the wood properties of an even-aged Scots pine forest. They found no statistical evidence that initial tree H and crown metrics, including width, area, volume, length, and height increment, related to the mean wood density of Scots pine trees. Instead, they found the mean branch angle was a significant predictor, explaining 31% of the WD variation between the trees.

Pyörälä et al. (2019) also showed the capability of stem taper and volume, derived from TLS, to assess the WD obtained from the Wood-X 4D Tomo device. Their study was conducted in Southern Finland and covered 52 Scots pine trees that were scanned in groups of 2–5 trees by applying adjustable scanning locations to maximize data coverage and manual tree extraction to ensure correct tree segmentation. The resulting correlations were –0.49 and –0.61 for stem taper and volume, respectively. For Norway spruce, however, the ΔH_{mean_tree} had a statistically significant, although rather low, correlation with WD_{mean_tree}, but no ALS metric was significant for predicting the WD_{mean_tree} of Norway spruce (Table 8). It is worth mentioning that the short time window in our study, focusing only on the last 15 growing seasons, might have limited the observed dependencies of WD_{mean_tree} with growth in tree H and crown metrics. In particular, WD is primarily influenced by tree age as a result of cambium maturation, and varies significantly from the corewood to outerwood (Wylie et al. 2019). In particular, our sample trees, with an average age of 64 years for the Scots pine and 84 years for the Norway spruce, were well into outerwood production, with high, stable WD. This age-related variability and the focus on a relatively recent period may have contributed to the findings of our study. However, other environmental factors, such as resource availability, precipitation, and temperature in the growing season, could have affected the annual variability in the WD, along with tree age (Rocha et al. 2019). While latewood production is generally consistent in Norway spruces, earlywood tends to vary more in response to environmental factors, with up to 80% of the variation in Norway spruce WD coming from differences in the annual rings, which were averaged out in our experimental design (Jyske et al. 2008).

At the plot level, the only significant correlation was found in Scots pine between WD_{mean_plot} and ΔCSA_{mean_plot}. This also appeared significant in explaining Scots pine WD_{mean_plot} variations, although to a lesser extent. This indicates that plots representing Scots pine with a greater increment in crown surface area tend to have higher WD_{mean_plot} values. In Norway spruce, however, none of the metrics showed a significant correlation or were significant predictors in the developed models. By comparison, Luther et al. (2014) were able to explain 40–53% of the variations in plot-level wood properties, including WD, in Canadian boreal forests. They utilized ALS-derived parameters extracted for each plot, such as tree height, fractal cover, and surface statistics. It is worth mentioning that the variability between sample plots caused by environmental conditions likely affected the observed relationship at the plot level. This has also been revealed by tree-level modeling when the inclusion of variability caused by the sample plots as a random effect improved the explanatory power of the models. Our experiment also did not find a significant relationship at the plot level between the standard deviations in growth in tree H and crown metrics with RW_{std_plot} and WD_{std_plot}, likely because of the presence of other influencing factors, such as soil fertility, water availability, and microclimatic conditions, which were not considered in the experiments. In addition, this might have been due to the low variability in WD_{mean_tree} because the sample trees were selected from among the dominant trees.

Generally, the results in Study **III** were likely affected by the rather narrow timeframe during which the growth was insufficient to adequately explain the wood properties of the trees. In addition, errors related to automatic tree segmentation present a significant source of uncertainty, particularly due to the occlusion. These can result in the omission of trees that are obscured beneath closed canopies, as well as the over- and under-segmentation of tree crowns, leading to inaccuracy in the estimated metrics. To date, automatic tree segmentation has been challenging in forests with complex structures, albeit it continues to improve in terms of both its accuracy and computational efficiency. In addition, the acquisition parameters, such as sensor specifications, the flight pattern, scan angle, and sampling rate, can also affect the point cloud properties (Cao et al. 2016; Socha et al. 2017b; Zhao et al. 2018). This becomes more important as repeated point clouds usually come from different instruments due to the continuous development of the technology and the various weather conditions at the acquisition times, which result in spatial inconsistencies (Duncanson and Dubayah 2018).

5 CONCLUSION

This thesis contains an amalgamation of Studies **I**–**III**, which explored the potential of utilizing LS point clouds as a monitoring approach for understanding forest dynamics and wood properties. Study **I** demonstrated the feasibility of using bi-temporal ALS data acquired over a 5-year period to detect changes in crown structure. To further explore its feasibility, Study **II** examined how well stem volume growth could be explained based on observations of crown characteristics and their development over time. In this study, we used a combination of Heli-ALS and TLS to provide a detailed reconstruction of trees, with the aim of mitigating the impact of occlusion that is typically associated with single-sensor acquisitions. The experiments showed that the ALS-derived crown metrics could explain 50%, 20%, and 6% of the observed variation in the ΔV of Scots pine, Norway spruce, and birches, respectively. For Scots pine, the most important predictors were the initial crown metrics, such as H, CP, and CA, which featured a correlation of 0.61–0.62 with the ΔV. By contrast, ΔCV emerged as the most important predictor for Norway spruces and birches, with correlations of 0.38–0.45 with ΔV. Building on these findings, Study **III** examined how mean annual increments of crown metrics, measured non-destructively using ALS, could be related to destructively sampled observations of WD and RW. Correlation analysis revealed stronger relationships for RW compared to WD with ALS-derived metrics during the last 15 growing seasons at the tree-level. Similar relationships were obtained when the individual tree observations were aggregated at the sample plot level. The inclusion of sample plot variability in linear mixed-effect modeling, however, enhanced the explanatory power of the models at the tree level. In particular, this approach explained 40–41% of the tree-level variability in RW, with mean annual increments in H being an important predictor, regardless of species.

This monitoring framework is important because the crown plays a key role in photosynthesis, its dimensions are associated with light interception capacity, and changes in its characteristics indicate shifts in ecophysiological functioning. Our findings support the existing knowledge on the capacity of ALS as an efficient tool for monitoring individual tree growth and provide ideas for possible application areas where such information needs to be obtained over large areas. The contribution to the current knowledge is further reflected in the observed association between crown development and wood properties, suggesting a potential trade-off between crown expansion and radial growth. However, reliable characterization of structural changes, especially in slow-growth boreal forests, remains a challenge. Moreover, the experiments conducted in this thesis focused solely on the contribution of initial crown characteristics and their development to growth allocation, while tree growth is also influenced by various other biophysical factors. These include resource availability (e.g., nutrients, water, and sunlight), competition among individuals, site productivity, and both stem-related and internal tree characteristics. Therefore, future research could benefit from incorporating complementary information on site conditions, competitive status, and other biophysical drivers to enhance the accuracy and ecological relevance of growth monitoring. More detailed tree measurements, in terms of spatial and temporal resolution, could advance our current knowledge of tree growth processes, representing the baseline for forest monitoring and growth simulation applications. Being capable of estimating stem volume growth based on observations of tree crowns, while predicting wood properties non-destructively, will improve forest biomass estimations and be of benefit in the sustainable use of forest resources. This research also encourages future studies to explore the impact of management intervention on tree growth and wood properties. Overall, this thesis has demonstrated the feasibility of bi-temporal LS to provide repetitive and non-destructive characterizations of individual trees in an attempt to indirectly monitor stem volume growth and wood properties.

REFERENCES

Aakala T, Fraver S, D'Amato AW, Palik BJ (2013) Influence of competition and age on tree growth in structurally complex old-growth forests in northern Minnesota, USA. For Ecol Manage 308: 128–135. https://doi.org/10.1016/j.foreco.2013.07.057

Ahmed S, Pretzsch H (2023) TLidar-based crown shape indicates tree ring pattern in Norway spruce (Picea abies (L.) H. Karst) trees across competition gradients. A modeling and methodological approach. Ecol Indic 148. https://doi.org/10.1016/j.ecolind.2023.110116

Ahmed S, Hilmers T, Uhl E, Jacobs M, Bohnhorst L, Kolisnyk B, del Río M, Pretzsch H (2024) Neighborhood competition modulates the link between crown structure and tree ring variability in monospecific and mixed forest stands. For Ecol Manage 560. https://doi.org/10.1016/j.foreco.2024.121839

Amarasekara H, Denne MP (2002) Effects of crown size on wood characteristics of Corsican pine in relation to definitions of juvenile wood, crown formed wood and core wood. Forestry 75: 51–61. https://doi.org/10.1093/forestry/75.1.51

Axelsson P (2000) DEM Generation from Laser Scanner Data Using adaptive TIN Models. Int Arch Photogramm Remote Sens 23: 110–117

Barrette J, Achim A, Auty D (2023) Impact of Intensive Forest Management Practices on Wood Quality from Conifers: Literature Review and Reflection on Future Challenges. Curr For Reports 9: 101–130. https://doi.org/10.1007/s40725-023-00181-6

Barton K (2015) Package "MuMIn." R Packag. version 1.15.1. https://cran.r-project.org/web/packages/MuMIn/MuMIn.pdf

Bates D, Mächler M, Bolker BM, Walker SC (2015) Fitting linear mixed-effects models using lme4. J Stat Softw 67. https://doi.org/10.18637/jss.v067.i01

Beekhuis J (1965) Crown depth of radiata pine in relation to stand density. New Zeal J For

10: 43–61

Bergsten U, Lindeberg J, Rindby A, Evans R (2001) Batch measurements of wood density on intact or prepared drill cores using x-ray microdensitometry. Wood Sci Technol 35: 435–452. https://doi.org/10.1007/s002260100106

Biging GS, Dobbertin M (1995) Evaluation of Competition Indices in Individual Tree Growth Models. For Sci 41: 360–377. https://doi.org/10.1093/forestscience/41.2.360

Biondi F, Qeadan F (2008) A theory-driven approach to tree-ring standardization: Defining the biological trend from expected basal area increment. Tree-Ring Res 64: 81–96. https://doi.org/10.3959/2008-6.1

Breiman L (2001) Random forests. Mach Learn 45: 5–32

Calders K, Adams J, Armston J, Bartholomeus H, Bauwens S, Bentley LP, Chave J, Danson FM, Demol M, Disney M, others (2020) Terrestrial laser scanning in forest ecology: Expanding the horizon. Remote Sens Environ 251: 112102

Cao L, Coops NC, Innes JL, Sheppard SRJ, Fu L, Ruan H, She G (2016) Estimation of forest biomass dynamics in subtropical forests using multi-temporal airborne LiDAR data. Remote Sens Environ 178: 158–171. https://doi.org/10.1016/j.rse.2016.03.012

Chen L, Xiang W, Wu H, Lei P, Zhang S, Ouyang S, Deng X, Fang X (2017) Tree growth traits and social status affect the wood density of pioneer species in secondary subtropical forest. Ecol Evol 7: 5366–5377. https://doi.org/10.1002/ece3.3110

Cohen J (2013) Statistical Power Analysis for the Behavioral Sciences. Routledge

Coomes DA, Allen RB (2007) Effects of size, competition and altitude on tree growth. J Ecol 95: 1084–1097. https://doi.org/10.1111/J.1365-2745.2007.01280.X

Coops NC (2015) Characterizing forest growth and productivity using remotely sensed data. Curr For Reports 1: 195–205. https://doi.org/10.1007/s40725-015-0020-x

Coops NC, Hilker T, Wulder MA, St-Onge B, Newnham G, Siggins A, Trofymow JA (2007) Estimating canopy structure of Douglas-fir forest stands from discrete-return LiDAR. Trees - Struct Funct 21: 295–310. https://doi.org/10.1007/s00468-006-0119-6

Dai W, Yang B, Liang X, Dong Z, Huang R, Wang Y, Li W (2019) Automated fusion of forest airborne and terrestrial point clouds through canopy density analysis. ISPRS J Photogramm Remote Sens 156: 94–107. https://doi.org/10.1016/J.ISPRSJPRS.2019.08.008

Demol M, Calders K, Krishna Moorthy SM, Van den Bulcke J, Verbeeck H, Gielen B (2021) Consequences of vertical basic wood density variation on the estimation of aboveground biomass with terrestrial laser scanning. Trees - Struct Funct 35: 671–684. https://doi.org/10.1007/s00468-020-02067-7

Downes GM, Drew DM (2008) Climate and growth influences on wood formation and utilisation. South For 70: 155–167. https://doi.org/10.2989/SOUTH.FOR.2008.70.2.11.539

Downes GM, Hudson IL, Raymond CA, Dean GH, Michell AJ, Schimleck LR, Evans R, Muneri A (1997) Sampling plantation eucalypts for wood and fibre properties. CSIRO publishing

Dubayah RO, Sheldon SL, Clark DB, Hofton MA, Blair JB, Hurtt GC, Chazdon RL (2010) Estimation of tropical forest height and biomass dynamics using lidar remote sensing at la Selva, Costa Rica. J Geophys Res Biogeosciences 115. https://doi.org/10.1029/2009JG000933

Duchesne I, Wilhelmsson L, Spangberg K (1997) Effects of in-forest sorting of Norway spruce (Picea abies) and Scots pine (Pinus sylvestris) on wood and fibre properties. Can J For Res 27: 790–795. https://doi.org/10.1139/x97-040

Duncanson L, Dubayah R (2018) Monitoring individual tree-based change with airborne lidar. Ecol Evol 8: 5079–5089. https://doi.org/10.1002/ece3.4075

Fish H, Lieffers VJ, Silins U, Hall RJ (2006) Crown shyness in lodgepole pine stands of varying stand height, density, and site index in the upper foothills of Alberta. Can J For Res 36: 2104–2111. https://doi.org/10.1139/X06-107

Frew MS, Evans DL, Londo HA, Cooke WH, Irby D (2016) Measuring douglas-fir crown growth with multitemporal LiDAR. For Sci 62: 200–212. https://doi.org/10.5849/forsci.14-062

Getzin S, Wiegand K (2007) Asymmetric tree growth at the stand level: Random crown patterns and the response to slope. For Ecol Manage 242: 165–174. https://doi.org/10.1016/j.foreco.2007.01.009

Givnish TJ (1988) Adaptation to sun and shade: a whole-plant perspective. Aust J Plant Physiol 15: 63–92. https://doi.org/10.1071/pp9880063

Hapfelmeier A, Hothorn T, Ulm K, Strobl C (2014) A new variable importance measure for random forests with missing data. Stat Comput 24: 21–34. https://doi.org/10.1007/S11222-012-9349-1/FIGURES/8

Hyyppä J, Hyyppä H, Leckie D, Gougeon F, Yu X, Maltamo M (2008) Review of methods of small-footprint airborne laser scanning for extracting forest inventory data in boreal forests. Int J Remote Sens 29: 1339–1366. https://doi.org/10.1080/01431160701736489

Ikonen VP, Peltola H, Wilhelmsson L, Kilpeläinen A, Väisänen H, Nuutinen T, Kellomäki S (2008) Modelling the distribution of wood properties along the stems of Scots pine (Pinus sylvestris L.) and Norway spruce (Picea abies (L.) Karst.) as affected by silvicultural management. For Ecol Manage 256: 1356–1371. https://doi.org/10.1016/j.foreco.2008.06.039

Isenburg M (2014) Rasterizing Perfect Canopy Height Models from LiDAR. rapidlasso GmbH

Isenburg M (2015) Use Buffers when Processing LiDAR in Tiles. rapidlasso GmbH. https://rapidlasso.com/2015/08/07/use-buffers-when-processing-lidar-in-tiles/

Jakubowski MK, Li W, Guo Q, Kelly M (2013) Delineating individual trees from lidar data: A comparison of vector- and raster-based segmentation approaches. Remote Sens 5: 4163–4186. https://doi.org/10.3390/rs5094163

Jevšenak J, Klisz M, Mašek J, Čada V, Janda P, Svoboda M, Vostarek O, Treml V, van der Maaten E, Popa A, Popa I, van der Maaten-Theunissen M, Zlatanov T, Scharnweber T, Ahlgrimm S, Stolz J, Sochová I, Roibu CC, Pretzsch H, Schmied G, Uhl E, Kaczka R, Wrzesiński P, Šenfeldr M, Jakubowski M, Tumajer J, Wilmking M, Obojes N, Rybníček M, Lévesque M, Potapov A, Basu S, Stojanović M, Stjepanović S, Vitas A, Arnič D, Metslaid S, Neycken A, Prislan P, Hartl C, Ziche D, Horáček P, Krejza J, Mikhailov S, Světlík J, Kalisty A, Kolář T, Lavnyy V, Hordo M, Oberhuber W, Levanič T, Mészáros I, Schneider L, Lehejček J, Shetti R, Bošeľa M, Copini P, Koprowski M, Sass-Klaassen U, Izmir ŞC, Bakys R, Entner H, Esper J, Janecka K, Martinez del Castillo E, Verbylaite R, Árvai M, de Sauvage JC, Čufar K, Finner M, Hilmers T, Kern Z, Novak K, Ponjarac R, Puchałka R, Schuldt B, Škrk Dolar N, Tanovski V, Zang C, Žmegač A, Kuithan C, Metslaid M, Thurm E, Hafner P, Krajnc L, Bernabei M, Bojić S, Brus R, Burger A, D'Andrea E, Đorem T, Gławęda M, Gričar J, Gutalj M, Horváth E, Kostić S, Matović B, Merela M, Miletić B, Morgós A, Paluch R, Pilch K, Rezaie N, Rieder J, Schwab N, Sewerniak P, Stojanović D, Ullmann T, Waszak N, Zin E, Skudnik M, Oštir K, Rammig A, Buras A (2024) Incorporating high-resolution climate, remote sensing and topographic data to map annual forest growth in central and eastern Europe. Sci Total Environ 913. https://doi.org/10.1016/j.scitotenv.2023.169692

Jung SE, Kwak DA, Park T, Lee WK, Yoo S (2011) Estimating Crown Variables of Individual Trees Using Airborne and Terrestrial Laser Scanners. Remote Sens 2011, Vol 3, Pages 2346-2363 3: 2346–2363. https://doi.org/10.3390/RS3112346

Jyske T, Mäkinen H, Saranpää P (2008) Wood density within Norway spruce stems. Silva Fenn 42: 439–455. https://doi.org/10.14214/sf.248

Kaitaniemi P, Lintunen A (2010) Neighbor identity and competition influence tree growth in Scots pine, Siberian larch, and silver birch. Ann For Sci 67: 604–604. https://doi.org/10.1051/forest/2010017

Kankare V, Vauhkonen J, Tanhuanpää T, Holopainen M, Vastaranta M, Joensuu M, Krooks A, Hyyppä J, Hyyppä H, Alho P, others (2014) Accuracy in estimation of timber assortments and stem distribution--A comparison of airborne and terrestrial laser scanning techniques. ISPRS J Photogramm Remote Sens 97: 89–97

Kankare V, Saarinen N, Pyörälä J, Yrttimaa T, Hynynen J, Huuskonen S, Hyyppä J, Vastaranta M (2022) Assessing the Dependencies of Scots Pine (Pinus sylvestris L.) Structural Characteristics and Internal Wood Property Variation. Forests 13. https://doi.org/10.3390/f13030397

Kassambara A (2023) rstatix: Pipe-Friendly Framework for Basic Statistical Tests Reference manual: rstatix.pdf

Khosravipour A, Skidmore AK, Isenburg M (2016) Generating spike-free digital surface models using LiDAR raw point clouds: A new approach for forestry applications. Int J Appl Earth Obs Geoinf 52: 104–114. https://doi.org/10.1016/j.jag.2016.06.005

Kim TK, Park JH (2019) More about the basic assumptions of t-test: Normality and sample size. Korean J Anesthesiol 72: 331–335. https://doi.org/10.4097/kja.d.18.00292

Krajicek J, Brinkman K, Gingrich S (1961) Crown competition-a measure of density. For Sci 7: 35–42

Krajnc L, Farrelly N, Harte AM (2019) The influence of crown and stem characteristics on timber quality in softwoods. For Ecol Manage 435: 8–17. https://doi.org/10.1016/j.foreco.2018.12.043

Kükenbrink D, Schneider FD, Leiterer R, Schaepman ME, Morsdorf F (2017) Quantification of hidden canopy volume of airborne laser scanning data using a voxel traversal algorithm. Remote Sens Environ 194: 424–436. https://doi.org/10.1016/J.RSE.2016.10.023

Kuprevicius A, Auty D, Achim A, Caspersen JP (2013) Quantifying the influence of live crown ratio on the mechanical properties of clear wood. Forestry 86: 361–369. https://doi.org/10.1093/forestry/cpt006

Laasasenaho J (1982) Taper curve and volume functions for pine, spruce and birch. Metsäntutkimuslaitos

Larson P (1969) Wood formation and the concept of wood quality. Yale Univ Sch For Bull 1–54

Liang X, Kankare V, Yu X, Hyyppä J, Holopainen M (2014) Automated stem curve measurement using terrestrial laser scanning. IEEE Trans Geosci Remote Sens 52: 1739–1748. https://doi.org/10.1109/TGRS.2013.2253783

Liang X, Kankare V, Hyyppä J, Wang Y, Kukko A, Haggrén H, Yu X, Kaartinen H, Jaakkola A, Guan F, others (2016) Terrestrial laser scanning in forest inventories. ISPRS J Photogramm Remote Sens 115: 63–77

Liang X, Hyyppä J, Kaartinen H, Lehtomäki M, Pyörälä J, Pfeifer N, Holopainen M, Brolly G, Francesco P, Hackenberg J, Huang H, Jo HW, Katoh M, Liu L, Mokroš M, Morel J, Olofsson K, Poveda-Lopez J, Trochta J, Wang D, Wang J, Xi Z, Yang B, Zheng G, Kankare V, Luoma V, Yu X, Chen L, Vastaranta M, Saarinen N, Wang Y (2018) International benchmarking of terrestrial laser scanning approaches for forest inventories. ISPRS J Photogramm Remote Sens 144: 137–179. https://doi.org/10.1016/J.ISPRSJPRS.2018.06.021

Listyanto T, Nichols JD (2009) A Review of Relationships Between Wood Quality and Silvicultural Practices. J Ilmu Kehutan 3: 116. https://doi.org/10.22146/jik.1513

Liu G, Wang J, Dong P, Chen Y, Liu Z (2018) Estimating individual tree height and diameter at breast height (DBH) from terrestrial laser scanning (TLS) data at plot level. Forests 9: 398

Luoma V, Saarinen N, Wulder MA, White JC, Vastaranta M, Holopainen M, Hyyppä J (2017) Assessing precision in conventional field measurements of individual tree attributes. Forests 8. https://doi.org/10.3390/f8020038

Luoma V, Yrttimaa T, Kankare V, Saarinen N, Pyörälä J, Kukko A, Kaartinen H, Hyyppä J, Holopainen M, Vastaranta M (2021) Revealing changes in the stem form and volume allocation in diverse boreal forests using two-date terrestrial laser scanning. Forests 12: 835

Luther JE, Skinner R, Fournier RA, Van Lier OR, Bowers WW, Coté JF, Hopkinson C, Moulton T (2014) Predicting wood quantity and quality attributes of balsam fir and black spruce using airborne laser scanner data. Forestry 87: 313–326. https://doi.org/10.1093/forestry/cpt039

Ma Q, Su Y, Tao S, Guo Q (2018) Quantifying individual tree growth and tree competition using bi-temporal airborne laser scanning data: a case study in the Sierra Nevada Mountains, California. Int J Digit Earth 11: 485–503. https://doi.org/10.1080/17538947.2017.1336578

Mäkelä A, Valentine HT (2006) Crown ratio influences allometric scaling in trees. Ecology 87: 2967–2972. https://doi.org/10.1890/0012-9658(2006)87[2967:CRIASI]2.0.CO;2

Mäkinen H, Colin F (1998) Predicting branch angle and branch diameter of Scots pine from usual tree measurements and stand structural information. Can J For Res 28: 1686–1696. https://doi.org/10.1139/cjfr-28-11-1686

Maltamo M, Eerikäinen K, Packalén P, Hyyppä J (2006) Estimation of stem volume using laser scanning-based canopy height metrics. Forestry 79: 217–229. https://doi.org/10.1093/forestry/cpl007

McRoberts RE, Bollandsås OM, Næsset E (2014) Modeling and Estimating Change. In: Forestry Applications of Airborne Laser Scanning: Concepts and Case Studies. Springer Netherlands, pp 293–313

Metz JÔ, Seidel D, Schall P, Scheffer D, Schulze ED, Ammer C (2013) Crown modeling by terrestrial laser scanning as an approach to assess the effect of aboveground intra- and interspecific competition on tree growth. For Ecol Manage 310: 275–288. https://doi.org/10.1016/J.FORECO.2013.08.014

Meyer F, Beucher S (1990) Morphological segmentation. J Vis Commun Image Represent 1: 21–46. https://doi.org/10.1016/1047-3203(90)90014-M

Mitchell KJ (1975) Dynamics and simulated yield of Douglas-fir. For Sci Monogr 17: 1–39. https://doi.org/10.20659/JFP.12.1_31

Moore JR, Cown DJ (2017) Corewood (Juvenile Wood) and Its Impact on Wood Utilisation. Curr For Reports 3: 107–118. https://doi.org/10.1007/s40725-017-0055-2

Næsset E (2004) Practical large-scale forest stand inventory using a small-footprint airborne scanning laser. Scand J For Res 19: 164–179. https://doi.org/10.1080/02827580310019257

Næsset E, Gobakken T (2005) Estimating forest growth using canopy metrics derived from airborne laser scanner data. Remote Sens Environ 96: 453–465. https://doi.org/10.1016/j.rse.2005.04.001

Nilsson M (1996) Estimation of tree heights and stand volume using an airborne lidar system. Remote Sens Environ 56: 1–7. https://doi.org/10.1016/0034-4257(95)00224-3

Noordermeer L, Økseter R, Ole Ørka H, Gobakken T, Næsset E, Bollandsås OM (2019) Classifications of forest change by using bitemporal airborne laser scanner data. Remote Sens 11. https://doi.org/10.3390/rs11182145

Novotny J, Navratilova B, Albert J, Cienciala E, Fajmon L, Brovkina O (2021) Comparison of spruce and beech tree attributes from field data, airborne and terrestrial laser scanning using manual and automatic methods. Remote Sens Appl Soc Environ 23: 100574. https://doi.org/10.1016/J.RSASE.2021.100574

Olejnik S, Algina J (2003) Generalized Eta and Omega Squared Statistics: Measures of Effect Size for Some Common Research Designs. Psychol Methods 8: 434–447. https://doi.org/10.1037/1082-989X.8.4.434

Osawa A, Ishizuka M, Kanazawa Y (1991) A profile theory of tree growth. For Ecol Manage 41: 33–63. https://doi.org/10.1016/0378-1127(91)90118-F

Ottorini J-M, Goff N Le, Cluzeau C (1996) Relationships between crown dimensions and stem development in Fraxinus excelsior. Can J For Res 26: 394–401

Panagiotidis D, Abdollahnejad A, Slavík M (2022) 3D point cloud fusion from UAV and TLS to assess temperate managed forest structures. Int J Appl Earth Obs Geoinf 112: 102917. https://doi.org/10.1016/J.JAG.2022.102917

Peltola H, Kilpeläinen A, Sauvala K, Räisänen T, Ikonen VP (2007) Effects of early thinning regime and tree status on the radial growth and wood density of scots pine. Silva Fenn 41: 489–505. https://doi.org/10.14214/sf.285

Peng C (2000) Growth and yield models for uneven-aged stands: Past, present and future. For Ecol Manage 132: 259–279. https://doi.org/10.1016/S0378-1127(99)00229-7

Pitkänen J, Maltamo M, Hyyppä J, Yu X (2004) Adaptive methods for individual tree detection on airborne laser based canopy height model. nternational Arch Photogramm Remote Sens Spat Inf Sci 36: 187–191

Pokharel B, Groot A, Pitt DG, Woods M, Dech JP (2016) Predictive modeling of black spruce (Picea mariana (Mill.) B.S.P.) wood density using stand structure variables derived from airborne LiDAR data in boreal forests of Ontario. Forests 7. https://doi.org/10.3390/f7120311

Polewski P, Yao W, Cao L, Gao S (2019) Marker-free coregistration of UAV and backpack LiDAR point clouds in forested areas. ISPRS J Photogramm Remote Sens 147: 307–318. https://doi.org/10.1016/J.ISPRSJPRS.2018.11.020

Pommerening A, Muszta A (2015) Methods of modelling relative growth rate. For Ecosyst 2. https://doi.org/10.1186/s40663-015-0029-4

Popescu SC, Wynne RH (2004) Seeing the trees in the forest: Using lidar and multispectral data fusion with local filtering and variable window size for estimating tree height. Photogramm Eng Remote Sensing 70: 589–604.

https://doi.org/10.14358/PERS.70.5.589

Popescu SC, Zhao K (2008) A voxel-based lidar method for estimating crown base height for deciduous and pine trees. Remote Sens Environ 112: 767–781. https://doi.org/10.1016/j.rse.2007.06.011

Pretzsch H (2021) Tree growth as affected by stem and crown structure. Trees - Struct Funct 35: 947–960. https://doi.org/10.1007/s00468-021-02092-0

Pretzsch H, Rais A (2016) Wood quality in complex forests versus even-aged monocultures: review and perspectives. Wood Sci Technol 50: 845–880. https://doi.org/10.1007/s00226-016-0827-z

Pretzsch H, Ahmed S, Jacobs M, Schmied G, Hilmers T (2022) Linking crown structure with tree ring pattern: methodological considerations and proof of concept. Trees - Struct Funct 36: 1349–1367. https://doi.org/10.1007/s00468-022-02297-x

Pyörälä J, Kankare V, Liang X, Saarinen N, Rikala J, Kivinen VP, Sipi M, Holopainen M, Hyyppä J, Vastaranta M (2019) Assessing log geometry and wood quality in standing timber using terrestrial laser-scanning point clouds. Forestry 92: 177–187. https://doi.org/10.1093/forestry/cpy044

R Core Team (2021) A language and environment for statistical computing. R Found. Stat. Comput. 3:https://www.R-project.org

Rapp JM, Silman MR, Clark JS, Girardin CAJ, Galiano D, Tito R, Doak DF (2012) Intra- and interspecific tree growth across a long altitudinal gradient in the Peruvian Andes. Ecology 93: 2061–2072. https://doi.org/10.1890/11-1725.1

Rocha MFV, Veiga TRLA, Soares BCD, de Araújo ACC, Carvalho AMM, Hein PRG (2019) Do the growing conditions of trees influence the wood properties? Floresta e Ambient 26. https://doi.org/10.1590/2179-8087.035318

Saarinen N, Kankare V, Vastaranta M, Luoma V, Pyörälä J, Tanhuanpää T, Liang X, Kaartinen H, Kukko A, Jaakkola A, others (2017) Feasibility of Terrestrial laser scanning for collecting stem volume information from single trees. ISPRS J Photogramm Remote Sens 123: 140–158

Schimleck L, Dahlen J, Apiolaza LA, Downes G, Emms G, Evans R, Moore J, Pâques L, Van den Bulcke J, Wang X (2019) Non-destructive evaluation techniques and what they tell us about wood property variation. Forests 10. https://doi.org/10.3390/f10090728

Schneider FD, Kükenbrink D, Schaepman ME, Schimel DS, Morsdorf F (2019) Quantifying 3D structure and occlusion in dense tropical and temperate forests using close-range LiDAR. Agric For Meteorol 268: 249–257. https://doi.org/10.1016/J.AGRFORMET.2019.01.033

Seidel D, Schall P, Gille M, Ammer C (2015) Relationship between tree growth and physical dimensions of Fagus sylvatica crowns assessed from terrestrial laser scanning. iForest - Biogeosciences For 8: 735. https://doi.org/10.3832/IFOR1566-008

Seifert T (2003) Integration von Holzqualität und Holzsortierung in behandlungssensitive Waldwachstumsmodelle. Technische Universität München

Sheppard J, Morhart C, Hackenberg J, Spiecker H (2017) Terrestrial laser scanning as a tool for assessing tree growth. iForest Biogeosciences For 10: 172–179

Sievänen R, Nikinmaa E, Nygren P, Ozier-Lafontaine H, Perttunen J, Hakula H (2000) Components of functional-structural tree models. Ann For Sci 57: 399–412. https://doi.org/10.1051/forest:2000131

Socha J, Pierzchalski M, Bałazy R, Ciesielski M (2017a) Modelling top height growth and site index using repeated laser scanning data. For Ecol Manage 406: 307–317

Socha J, Pierzchalski M, Bałazy R, Ciesielski M (2017b) Modelling top height growth and site index using repeated laser scanning data. For Ecol Manage 406: 307–317. https://doi.org/10.1016/J.FORECO.2017.09.039

Soininen V, Kukko A, Yu X, Kaartinen H, Luoma V, Saikkonen O, Holopainen M, Matikainen L, Lehtomäki M, Hyyppä J (2022) Predicting Growth of Individual Trees Directly and Indirectly Using 20-Year Bitemporal Airborne Laser Scanning Point Cloud Data. Forests 13. https://doi.org/10.3390/f13122040

Soininen V, Hyyppä E, Muhojoki J, Luoma V, Kaartinen H, Lehtomäki M, Kukko A, Hyyppä J (2024) Accuracy comparison of terrestrial and airborne laser scanning and manual measurements for stem curve-based growth measurements of individual trees. Sci Remote Sens 9. https://doi.org/10.1016/j.srs.2024.100125

Srinivasan S, Popescu SC, Eriksson M, Sheridan RD, Ku N-W (2015) Terrestrial laser scanning as an effective tool to retrieve tree level height, crown width, and stem diameter. Remote Sens 7: 1877–1896

Stephenson NL, Das AJ, Condit R, Russo SE, Baker PJ, Beckman NG, Coomes DA, Lines ER, Morris WK, Rüger N, Álvarez E, Blundo C, Bunyavejchewin S, Chuyong G, Davies SJ, Duque Á, Ewango CN, Flores O, Franklin JF, Grau HR, Hao Z, Harmon ME, Hubbell SP, Kenfack D, Lin Y, Makana JR, Malizia A, Malizia LR, Pabst RJ, Pongpattananurak N, Su SH, Sun IF, Tan S, Thomas D, Van Mantgem PJ, Wang X, Wiser SK, Zavala MA (2014) Rate of tree carbon accumulation increases continuously with tree size. Nature 507: 90–93. https://doi.org/10.1038/nature12914

Swenson NG, Enquist BJ (2007) Ecological and evolutionary determinants of a key plant functional trait: Wood density and its community-wide variation across latitude and elevation. Am J Bot 94: 451–459. https://doi.org/10.3732/ajb.94.3.451

Terryn L, Calders K, Bartholomeus H, Bartolo RE, Brede B, D'hont B, Disney M, Herold M, Lau A, Shenkin A, Whiteside TG, Wilkes P, Verbeeck H (2022) Quantifying tropical forest structure through terrestrial and UAV laser scanning fusion in Australian rainforests. Remote Sens Environ 271: 112912. https://doi.org/10.1016/J.RSE.2022.112912

Tompalski P, Coops NC, White JC, Goodbody TRH, Hennigar CR, Wulder MA, Socha J, Woods ME (2021) Estimating Changes in Forest Attributes and Enhancing Growth Projections: a Review of Existing Approaches and Future Directions Using Airborne

3D Point Cloud Data. Curr For Reports 7: 1–24. https://doi.org/10.1007/S40725-021-00135-W/FIGURES/5

Triola MF, Goodman WM, Law R, Labute G (2006) Elementary statistics (p. 794). Read Pearson/Addison-Wesley

Vaglio Laurin G, Ding J, Disney M, Bartholomeus H, Herold M, Papale D, Valentini R (2019) Tree height in tropical forest as measured by different ground, proximal, and remote sensing instruments, and impacts on above ground biomass estimates. Int J Appl Earth Obs Geoinf 82: 101899. https://doi.org/10.1016/J.JAG.2019.101899

Valentine HT, Mäkelä A, Green EJ, Amateis RL, Mäkinen H, Ducey MJ (2012) Models relating stem growth to crown length dynamics: Application to loblolly pine and Norway spruce. Trees - Struct Funct 26: 469–478. https://doi.org/10.1007/S00468-011-0608-0/FIGURES/7

Van Leeuwen M, Hilker T, Coops NC, Frazer G, Wulder MA, Newnham GJ, Culvenor DS (2011) Assessment of standing wood and fiber quality using ground and airborne laser scanning: A review. For Ecol Manage 261: 1467–1478. https://doi.org/10.1016/j.foreco.2011.01.032

Vastaranta M, Holopainen M, Yu X, Hyyppä J, Mäkinen A, Rasinmäki J, Melkas T, Kaartinen H, Hyyppä H (2011) Effects of individual tree detection error sources on forest management planning calculations. Remote Sens 3: 1614–1626. https://doi.org/10.3390/rs3081614

Vastaranta M, Wulder MA, White JC, Pekkarinen A, Tuominen S, Ginzler C, Kankare V, Holopainen M, Hyyppä J, Hyyppä H (2013) Airborne laser scanning and digital stereo imagery measures of forest structure: Comparative results and implications to forest mapping and inventory update. Can J Remote Sens 39: 382–395. https://doi.org/10.5589/m13-046

Vepakomma U, St-Onge B, Kneeshaw D (2011) Response of a boreal forest to canopy opening: Assessing vertical and lateral tree growth with multi-temporal lidar data. Ecol Appl 21: 99–121. https://doi.org/10.1890/09-0896.1

Wang Y, Lehtomäki M, Liang X, Pyörälä J, Kukko A, Jaakkola A, Liu J, Feng Z, Chen R, Hyyppä J (2019) Is field-measured tree height as reliable as believed – A comparison study of tree height estimates from field measurement, airborne laser scanning and terrestrial laser scanning in a boreal forest. ISPRS J Photogramm Remote Sens 147: 132–145. https://doi.org/10.1016/j.isprsjprs.2018.11.008

Wehr A, Lohr U (1999) Airborne laser scanning—an introduction and overview. ISPRS J Photogramm Remote Sens 54: 68–82. https://doi.org/https://doi.org/10.1016/S0924-2716(99)00011-8

Weiner J (2004) Allocation, plasticity and allometry in plants. Perspect Plant Ecol Evol Syst 6: 207–215. https://doi.org/10.1078/1433-8319-00083

Weiskittel AR, Hann DW, Kershaw JA, Vanclay JK (2011) Forest Growth and Yield Modeling. For Growth Yield Model. https://doi.org/10.1002/9781119998518

Wensel LC, Meerschaert WJ, Biging GS (1987) Tree height and diameter growth models for Northern California conifers. Hilgardia 55: 1–20. https://doi.org/10.3733/hilg.v55n08p020

White JC, Tompalski P, Vastaranta M, Wulder MA, Saarinen N, Stepper C, Coops NC (2017) A model development and application guide for generating an enhanced forest inventory using airborne laser scanning data and an area-based approach. 1–48

Wylie RRM, Woods ME, Dech JP (2019) Estimating stand age from airborne laser scanning data to improve models of black spruce wood density in the boreal forest of Ontario. Remote Sens 11. https://doi.org/10.3390/rs11172022

Yrttimaa T, Saarinen N, Kankare V, Liang X, Hyyppä J, Holopainen M, Vastaranta M (2019) Investigating the feasibility of multi-scan terrestrial laser scanning to characterize tree communities in southern boreal forests. Remote Sens 11: 1423

Yrttimaa T, Saarinen N, Kankare V, Viljanen N, Hynynen J, Huuskonen S, Holopainen M, Hyyppä J, Honkavaara E, Vastaranta M (2020a) Multisensorial close-range sensing generates benefits for characterization of managed scots pine (Pinus sylvestris L.) stands. ISPRS Int J Geo-Information 9. https://doi.org/10.3390/ijgi9050309

Yrttimaa T, Saarinen N, Kankare V, Hynynen J, Huuskonen S, Holopainen M, Hyyppä J, Vastaranta M (2020b) Performance of terrestrial laser scanning to characterize managed Scots pine (Pinus sylvestris L.) stands is dependent on forest structural variation. ISPRS J Photogramm Remote Sens 168: 277–287. https://doi.org/10.1016/J.ISPRSJPRS.2020.08.017

Yrttimaa T, Luoma V, Saarinen N, Kankare V, Junttila S, Holopainen M, Hyyppä J, Vastaranta M (2022) Exploring tree growth allometry using two-date terrestrial laser scanning. For Ecol Manage 518: 120303. https://doi.org/10.1016/J.FORECO.2022.120303

Yrttimaa T, Junttila S, Hyyppä J, Holopainen M, Wulder MA, Vastaranta M (2024) Quantifying architectural uniqueness of Scots pine trees using terrestrial laser scanning: toward individual tree fingerprinting. For An Int J For Res. https://doi.org/10.1093/forestry/cpae058

Yu X, Hyyppä J, Kaartinen H, Maltamo M (2004) Automatic detection of harvested trees and determination of forest growth using airborne laser scanning. Remote Sens Environ 90: 451–462. https://doi.org/10.1016/j.rse.2004.02.001

Yun T, Cao L, An F, Chen B, Xue L, Li W, Pincebourde S, Smith MJ, Eichhorn MP (2019) Simulation of multi-platform LiDAR for assessing total leaf area in tree crowns. Agric For Meteorol 276–277: 107610. https://doi.org/10.1016/J.AGRFORMET.2019.06.009

Zhang Z (1994) Iterative point matching for registration of free-form curves and surfaces. Int J Comput Vis 13: 119–152. https://doi.org/10.1007/BF01427149/METRICS

Zhao K, Suarez JC, Garcia M, Hu T, Wang C, Londo A (2018) Utility of multitemporal lidar for forest and carbon monitoring: Tree growth, biomass dynamics, and carbon flux. Remote Sens Environ 204: 883–897. https://doi.org/10.1016/j.rse.2017.09.007

Zimmerman DW (1994) A note on the influence of outliers on parametric and nonparametric tests. J Gen Psychol 121: 391–401. https://doi.org/10.1080/00221309.1994.9921213